

# STAR-RIS Assisted Full-Duplex Communication Networks

Abdelhamid Salem, *Member, IEEE*, and Kai-Kit Wong, *Fellow, IEEE*, Chan-Byoung  
Chae, *Fellow, IEEE* and Yangyang Zhang

## Abstract

Different from conventional reconfigurable intelligent surfaces (RIS), a recent innovation called simultaneous transmitting and reflecting reconfigurable intelligent surface (STAR-RIS) has emerged, aimed at achieving complete 360-degree coverage in communication networks. Additionally, full-duplex (FD) technology is recognized as a potent approach for enhancing spectral efficiency by enabling simultaneous transmission and reception within the same time and frequency resources. In this study, we investigate the performance of a STAR-RIS-assisted FD communication system. The STAR-RIS is strategically placed at the cell-edge to facilitate communication for users located in this challenging region, while cell-center users can communicate directly with the FD base station (BS). We employ a non-orthogonal multiple access (NOMA) pairing scheme and account for system impairments, such as self-interference at the BS and imperfect successive interference cancellation (SIC). We derive closed-form expressions for the ergodic rates in both the up-link and down-link communications and extend our analysis to bidirectional communication between cell-center and cell-edge users. Furthermore, we formulate an optimization problem aimed at maximizing the ergodic sum-rate. This optimization involves adjusting the amplitudes and phase-shifts of the STAR-RIS elements and allocating total transmit power efficiently. To gain deeper insights into the achievable rates of STAR-RIS-aided FD systems, we explore the impact of various system parameters through numerical results.

Abdelhamid Salem is with the department of Electronic and Electrical Engineering, University College London, London, UK, (emails: a.salem@ucl.ac.uk).

Kai-Kit Wong is with the department of Electronic and Electrical Engineering, University College London, London, UK, (email: kai-kit.wong@ucl.ac.uk). Kai-Kit Wong is also affiliated with Yonsei University, Seoul, Korea.

Chan-Byoung Chae is with the School of Integrated Technology, Yonsei University, Seoul, 03722 Korea (e-mail: cbchae@yonsei.ac.kr).

Yangyang Zhang is with Kuang-Chi Science Ltd., Hong Kong, SAR, China.

## Index Terms

Full-duplex, STAR-RIS, NOMA, Ergodic Sum-rate.

### I. INTRODUCTION

Reconfigurable intelligent surface (RIS) has been recognized as a key technique for the upcoming sixth-generation (6G) wireless communication networks [1]–[4]. The conventional RIS is equipped with controllable reflecting elements, that can adjust the phase shifts of the incident signals to improve the received signals' quality [1]–[3]. Therefore, RIS can make the propagation environments smart and controllable. The performance of RIS has been extensively studied in the literature for different applications [5]–[8]. However, the conventional RIS can provide only half-space coverage, and thus the transmitters and receivers should be located on the same side of the aided RIS. To tackle this issue and extend the RIS coverage area, simultaneous transmitting and reflecting RIS (STAR-RIS) has been proposed recently [9]–[20]. STAR-RIS can transmit and reflect the signals into both sides of the surface, and thus it can provide full-space coverage. The concept of STAR-RIS was introduced and discussed in [9], [10] where three operating protocols for the STAR-RIS have been proposed, namely, energy splitting (ES), mode switching (MS), and time switching (TS). In ES, the energy of the incident wave on each STAR-RIS element is split into energy of the transmitted signals and energy of the reflected signals, and in the MS protocol, the STAR-RIS elements are divided into two groups: one group operates in transmission mode, while the other group operates in reflecting mode. Also, in the TS protocol, the STAR-RIS elements periodically switch between transmission mode and reflection mode in different time slots. The authors in [11] analyzed the ergodic rates of the STAR-RIS-assisted non-orthogonal multiple access (NOMA) systems, where a STAR-RIS was implemented to assist the cell-edge users. In [12], the performance of STAR-RIS-aided NOMA systems was studied to support low-latency communications. In [13], an analytical expression of the coverage probability for a STAR-RIS aided massive multiple input multiple output (mMIMO) communication systems was derived. Further work in [14] provided an analytical framework of the coverage probability and ergodic rate of STAR-RIS assisted NOMA multi-cell networks. A power minimization problem for STAR-RIS-aided up-link NOMA systems was considered in

[15]. The authors in [16] considered the energy efficiency of a STAR-RIS-empowered MIMO-NOMA systems. In [17], an approximate analytical expression of the ergodic rate of STAR-RIS-aided NOMA downlink communication system was derived. A new joint optimization problem to maximize the achievable sum rate of STAR-RIS NOMA system has been formulated and solved in [18]. In [19], a STAR-RIS-assisted two-user communication systems has been considered for both orthogonal multiple access (OMA) and NOMA schemes. The performance of STAR-RIS aided NOMA systems over Rician fading channels has been analyzed in [20].

Moreover, full-duplex (FD) technique allows the communication nodes to transmit and receive data simultaneously in the same frequency and time resources [21]–[23]. Thus, FD can enhance the achievable rates and provide a more flexible use of the spectrum. Interestingly, the performance of RIS-aided FD communication systems has been considered recently in several works [24]–[30]. For instance, in [24], a passive beamforming design for RIS-assisted FD communication was investigated, where a FD access point communicates with an uplink (UL) user and a downlink (DL) user simultaneously with the help of RIS. In [25], the resource allocation design for RIS-assisted FD communication systems was considered. In [26], the authors proposed deploying an RIS in a FD two-way communication systems to provide signal coverage for the users in the dead areas. A joint beamforming design for a RIS-assisted FD communication systems was considered in [27], where the total transmit power was minimized by optimizing the active beamforming at the transmitter and passive beamforming at the RIS. In [28] a RIS-aided FD communication system has been analyzed, where a FD-BS communicates with FD-users through a dedicated RIS.

Accordingly, this work considers a STAR-RIS aided FD communication system, where the FD-BS serves the cell-center users and cell-edge users using NOMA pairing scheme. The BS communicates with the cell-edge users via passive STAR-RIS, while the cell-center users can communicate directly with the BS. We concentrate on the ergodic rate analysis, the STAR-RIS design and the power allocation, by employing statistical channel state information (CSI). We first derive closed-form expressions for the ergodic rates of the DL and UL users in the system. Then, we apply our analysis to the bidirectional communication between the cell-center and cell-edge users. In addition, the sum-rate of both scenarios are maximized by optimizing the

STAR-RIS reflection coefficients and the power allocation between the DL and UL users. For clarity, the main contributions are listed as follows:

1) We investigate the performance of STAR-RIS aided FD-BS communication systems, where the STAR-RIS is implemented to assist the cell-edge users.

2) New closed-form analytical expressions for the ergodic rates of the DL and UL users are derived when the cell-center users are paired with the cell-edge users under Rician fading channels. This channel model is more general but also very challenging to analyze. Also, the impact of imperfect successive interference cancellation (SIC) and all interferences including the self interference at the FD-BS are considered in the analysis. The derived ergodic rate expressions are explicit and provide several important practical design insights.

3) Besides many applications, our analysis is then applied to the bidirectional communication scenario, where the UL cell-center user and UL cell-edge user communicate with the DL cell-edge user and DL cell-center user, respectively. Simple closed form expressions for the ergodic rates of the DL users are derived.

4) We formulate and solve a sum-rate maximization problem by jointly optimizing the phase shifts and amplitudes at the STAR-RIS and the power allocation coefficients. To efficiently solve this challenging problem, we divide the main problem into two sub-problems, i.e., phase shift and amplitude optimization, and power allocation optimization, then we solve them alternatively. In addition, based on the derived rate expressions, we introduce sub-optimal designs of the STAR-RIS and the power allocation schemes.

5) Monte-Carlo simulations are performed to validate the analytical expressions. Then, the impact of several parameters on the system performance are investigated.

The results in this work show that increasing the transmit signal to noise ratio (SNR) always enhances the achievable users' rates, and using a large number of STAR-RIS units improves the performance of the cell-edge users. In addition, high power should be allocated to the DL users to overcome the interference caused by the UL users. The imperfect SIC degrades the achievable rates of the DL cell-center user and the UL cell-edge user, while a high variance of the residual self interference at the BS leads to degrade the performance of the UL users significantly.

Next, in Section II the system model is presented. In Section III, we derive the ergodic rates

of the DL and UL users in the NOMA pairing scheme. The ergodic rates of the DL users in the bidirectional communication scenario are provided in Section IV. Section V discusses the optimal system design. Section VI depicts our numerical results. Our main conclusions are summarized in Section VII.

## II. SYSTEM MODEL

We consider a STAR-RIS-aided multiuser communication system operating in FD mode, as shown in Fig 1. The FD-BS is deployed at the cell-center with a coverage radius  $R_t$ , while a STAR-RIS with  $N$  reconfigurable elements is deployed at the cell-edge with a coverage radius  $R_r$ . Based on the BS and the STAR-RIS deployments, the total coverage area  $R_t$  is divided into two areas, i.e., the cell-center region with radius  $R$ , and the cell-edge region with radius  $R_r$ . The BS is assumed to be equipped with two antennas, one for transmission and one for reception, and each user in the system is equipped with a single antenna. Number of the UL and DL users in the cell-center region are  $K_{cu}$  and  $K_{cd}$ , respectively, where  $K_{cu} + K_{cd} = K_c$ , while number of the UL and DL users in the cell-edge region are  $K_{eu}$  and  $K_{ed}$ , respectively, where  $K_{eu} + K_{ed} = K_e$ . The users are uniformly distributed in the area, where the cell-center users can communicate directly with the BS, while the cell-edge users transmit and receive their messages through the STAR-RIS. It is known that the STAR-RIS is most likely to be installed on the buildings, and hence it can create channels dominated by the line-of-sight (LoS) path along with the scatterers. Thus, Rician fading model is considered for the STAR-RIS related channels. On the other hand, Rayleigh fading is assumed for the BS to users and user to user channels due to the wealth of scatterers.

### A. STAR-RIS Protocol

In this work, the ES protocol has been implemented at the STAR-RIS. In the ES scheme, the signal incident upon each SAR-RIS element is split into transmitted and reflected signals, with ES coefficients (also named amplitude coefficients)  $\rho_n^r$  and  $\rho_n^t$  ( $\rho_n^r + \rho_n^t \leq 1$ ). Thus, the transmission ( $t$ ) and reflection ( $r$ ) coefficient matrices of the STAR-RIS can be written as  $\Theta_k = \text{diag}(\rho_1^k \theta_1^k, \dots, \rho_N^k \theta_N^k)$ ,  $k \in \{t, r\}$ , where  $\theta_n^k = e^{j\phi_n^k}$ ,  $\rho_n^k \in [0, 1]$ ,  $\rho_n^k > 1$  and  $|\theta_n^k| = 1$ .

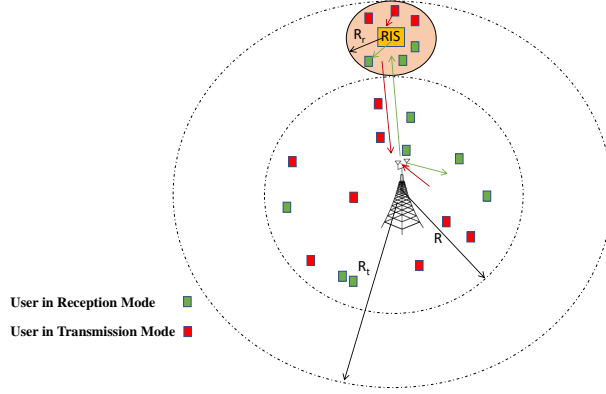


Figure 1. A STAR-RIS assisted FD communication system.

### III. DATA TRANSMISSION AND ERGODIC RATES

In the system model under consideration, the FD-BS serves the DL and UL users by employing NOMA-pairing scheme as follows. In each time slot, the BS transmits signals to two DL users, a DL cell-center user (near/strong user), and a DL cell-edge user (far/weak user), and in the same time slot, the BS receives signals from two UL users, an UL cell-center user (near/strong user), and an UL cell-edge user (far/weak user). It is worth mentioning that, the users benefit from NOMA transmissions over OMA transmission by satisfying the necessary condition that the achievable rate of NOMA ( $R_{u_i}^{NOMA}$ ) is larger than that of OMA, ( $R_{u_i}^{OMA}$ ). This condition can be expressed as,  $\gamma_{u_i}^{NOMA} > \sqrt{1 + \gamma_{u_i}^{OMA}} - 1$ , where  $\gamma_{u_i}$  is the signal to interference and noise ratio (SINR) at user  $i$ .

#### A. DL

In the DL mode, in a given time slot, the BS transmits the following superimposed signal

$$s = \sum_{i=1}^2 \sqrt{\alpha_i} x_{u_{id}}, \quad (1)$$

where  $\alpha_i$  is the power allocation coefficient of user  $i$  with  $\alpha_1 + \alpha_2 = 1$ , and  $x_{u_{id}}$  is the information signal of user  $i$  with unit variance.

1) *Cell-center/strong user*: The received signal at the DL cell-center/strong user (user 1) can be expressed as

$$y_{u_{1d}} = \sum_{i=1}^2 \sqrt{P_{b_i}} x_{u_{1d}} \left( \sqrt{l_{b,u_{1d}}^{-m}} h_{b,u_{1d}} + \sqrt{l_{b,r}^{-m} l_{r,u_{1d}}^{-m}} \mathbf{g}_{r,u_{1d}} \Theta_t \mathbf{g}_{b,r} \right) + I_{u_{1d}} + n_{u_{1d}}, \quad (2)$$

where  $P_{b_i} = \alpha_i P_b$ ,  $P_b$  is the BS transmit power,  $\alpha_1, \alpha_2$  are the power coefficients of the cell-center and cell-edge users, respectively, with  $\alpha_1 < \alpha_2$ ,  $l_{b,u_{1d}}^{-m}, l_{b,r}^{-m}, l_{r,u_{1d}}^{-m}$  represent the path-loss between the BS and DL cell-center user, BS and RIS, RIS and DL cell-center user, respectively,  $m$  is the path-loss exponent,  $h_{b,u_{1d}} \sim CN(0, 1)$  is the channel between the BS and DL cell-center user, and  $\mathbf{g}_{r,u_{1d}} = \left( \sqrt{\frac{\kappa_{r,u_{1d}}}{\kappa_{r,u_{1d}}+1}} \bar{\mathbf{g}}_{r,u_{1d}} + \sqrt{\frac{1}{\kappa_{r,u_{1d}}+1}} \tilde{\mathbf{g}}_{r,u_{1d}} \right) \in \mathbb{C}^{1 \times N}$ ,  $\mathbf{g}_{b,r} = \left( \sqrt{\frac{\kappa_{b,r}}{\kappa_{b,r}+1}} \bar{\mathbf{g}}_{b,r} + \sqrt{\frac{1}{\kappa_{b,r}+1}} \tilde{\mathbf{g}}_{b,r} \right) \in \mathbb{C}^{N \times 1}$  are the channel vectors between the DL cell-center user and the RIS, and the BS and the RIS, respectively,  $\kappa_{r,u_{1d}}$  and  $\kappa_{b,r}$  are the Rician factors,  $\bar{\mathbf{g}}_{r,u_{1d}}$  and  $\bar{\mathbf{g}}_{b,r}$  are the LoS components and  $\tilde{\mathbf{g}}_{r,u_{1d}}, \tilde{\mathbf{g}}_{b,r}$  are the non-LoS (NLoS) components,  $n_{u_{1d}}$  is the additive white Gaussian noise (AWGN) at the user,  $n_{u_{1d}} \sim CN(0, \sigma_{u_{1d}}^2)$ , and  $I_{u_{1d}}$  is the interference caused by the UL users and given by

$$I_{u_{1d}} = \underbrace{\sqrt{p_{u_{1u}}} x_{u_{1u}} \left( \sqrt{l_{u_{1d},u_{1u}}^{-m}} h_{u_{1d},u_{1u}} + \sqrt{l_{r,u_{1u}}^{-m} l_{r,u_{1d}}^{-m}} \mathbf{g}_{r,u_{1d}} \Theta_t \mathbf{g}_{r,u_{1u}} \right)}_{\text{interference from UL cell center user}} + \underbrace{\sqrt{p_{u_{2u}}} l_{r,u_{2u}}^{-m} l_{r,u_{1d}}^{-m} \mathbf{g}_{r,u_{1d}} \Theta_t \mathbf{g}_{r,u_{2u}} x_{u_{2u}}}_{\text{interference from UL cell edge user}}$$

where  $p_{u_{1u}}, p_{u_{2u}}, x_{u_{1u}}, x_{u_{2u}}$  are the transmit powers and signals of the UL cell-center and cell-edge users,  $h_{u_{1d},u_{1u}} \sim CN(0, 1)$  is the channel between the cell-center users in UL and DL modes, and  $\mathbf{g}_{r,u_{1u}} = \left( \sqrt{\frac{\kappa_{r,u_{1u}}}{\kappa_{r,u_{1u}}+1}} \bar{\mathbf{g}}_{r,u_{1u}} + \sqrt{\frac{1}{\kappa_{r,u_{1u}}+1}} \tilde{\mathbf{g}}_{r,u_{1u}} \right)$ ,  $\mathbf{g}_{r,u_{2u}} = \left( \sqrt{\frac{\kappa_{r,u_{2u}}}{\kappa_{r,u_{2u}}+1}} \bar{\mathbf{g}}_{r,u_{2u}} + \sqrt{\frac{1}{\kappa_{r,u_{2u}}+1}} \tilde{\mathbf{g}}_{r,u_{2u}} \right)$  are the channel vectors between the UL cell-center user and the RIS, and the UL cell-edge user and the RIS, respectively.

The SINR at the DL cell-center user can be written as

$$\gamma_{u_{1d}} = \frac{P_{b_1} A_{u_{1d}}}{\Xi P_{b_2} A_{u_{1d}} + p_{u_{1u}} C_{u_{1d}} + p_{u_{2u}} D_{u_{1d}} + \sigma_{u_{1d}}^2}, \quad (3)$$

where

$$A_{u_{1d}} = \left| \sqrt{l_{b,u_{1d}}^{-m}} h_{b,u_{1d}} + \sqrt{l_{b,r}^{-m} l_{r,u_{1d}}^{-m}} \mathbf{g}_{r,u_{1d}} \Theta_t \mathbf{g}_{b,r} \right|^2,$$

$$C_{u_{1d}} = \left| \sqrt{l_{u_{1d},u_{1u}}^{-m}} h_{u_{1d},u_{1u}} + \sqrt{l_{r,u_{1u}}^{-m} l_{u_{r,u_{1d}}}^{-m}} \mathbf{g}_{r,u_{1d}} \Theta_t \mathbf{g}_{r,u_{1u}} \right|^2,$$

$D_{u_{1u}} = l_{r,u_{2u}}^{-m} l_{r,u_{1d}}^{-m} |\mathbf{g}_{r,u_{1d}} \Theta_t \mathbf{g}_{r,u_{2u}}|^2$ , and  $0 \leq \Xi \leq 1$  is the fractional error factor that corresponds to a fraction of the power that remains as interference due to imperfect SIC. In NOMA pairing scheme, the rate for the strong user to detect the weak user signal,  $R_{u_{1d} \rightarrow u_{2d}}$ , should be larger than or equal to the rate of the weak user  $R_{u_{2d}}$ .

**Theorem 1.** *The ergodic DL rate of the cell-center user in passive STAR-RIS-aided FD communication systems under Rician fading channels can be calculated by*

$$\mathcal{E}[R_{u_{1d}}] \approx \log_2 \left( 1 + \frac{P_{b_1} x_{1u_{1d}}}{\Xi P_{b_2} x_{1u_{1d}} + p_{u_{1u}} y_{1u_{1d}} + p_{u_{2u}} y_{2u_{1d}} + \sigma_{u_{1d}}^2} \right) \quad (4)$$

where

$$x_{1u_{1d}} = \frac{2(1+R)^{-m}(-1+R^2+mR(1+R)+(1+R)^m)}{(m-2)(m-1)R^2} + l_{b,r}^{-m} \Upsilon(\varpi_{b,r}^{r,u_{1d}} \xi_1 + \hat{\varpi}_{b,r}^{r,u_{1d}}), \quad (5)$$

$$y_{1u_{1d}} = (\varrho + \Upsilon^2(\varpi_{r,u_{1u}}^{r,u_{1d}} \xi_2 + \hat{\varpi}_{r,u_{1u}}^{r,u_{1d}})) \quad (6)$$



$$y_{2_{u_{1d}}} = \frac{2(1+R_r)^{-m}(-1+R_r^2+mR_r(1+R_r)+(1+R_r)^m)\Upsilon(\widehat{\varpi}_{r,u_{2u}}^{r,u_{1d}}\xi_3+\widehat{\varpi}_{r,u_{2u}}^{r,u_{1d}})}{(m-2)(m-1)R_r^2} \quad (7)$$

where  $\varpi_y^x = \frac{\kappa_x}{\kappa_x+1}\frac{\kappa_y}{\kappa_y+1}$ ,  $\widehat{\varpi}_y^x = \frac{\kappa_x}{\kappa_x+1}\frac{\sum_{n=1}^N|\rho_n^k|^2}{\kappa_y+1} + \frac{\kappa_y}{\kappa_y+1}\frac{\sum_{n=1}^N|\rho_n^k|^2}{\kappa_x+1} + \frac{1}{\kappa_x+1}\frac{\sum_{n=1}^N|\rho_n^k|^2}{\kappa_y+1}$ ,  
 $\Upsilon = \sum_{j=1}^C H_j (1+(Rr_j+R))^{-m} \frac{2(Rr_j+R)}{\pi R^2} \cos^{-1}\left(\frac{1}{(Rr_j+R)}\left(r_1 + \frac{((Rr_j+R)^2-r_1^2)}{2(R+r_1)}\right)\right)$ ,  
 $\varrho = \left(\frac{2}{(2-3m+m^2)R^2} - \frac{2F(\{\frac{1}{2}, -1+\frac{m}{2}, -\frac{1}{2}+\frac{m}{2}\}, \{\frac{-1}{2}, 1\}, 4R^2)}{(2-3m+m^2)R^2} - F(\{\frac{3}{2}, \frac{1}{2}+\frac{m}{2}, \frac{m}{2}\}, \{\frac{1}{2}, 3\}, 4R^2)\right.$   
 $\left. + \frac{64mRF(\{2, \frac{1}{2}+\frac{m}{2}, 1+\frac{m}{2}\}, \{\frac{3}{2}, \frac{7}{2}\}, 4R^2)}{15\pi} - \frac{64mRF(\{2, \frac{1}{2}+\frac{m}{2}, 1+\frac{m}{2}\}, \{\frac{5}{2}, \frac{5}{2}\}, 4R^2)}{9\pi}\right)$  and  $F(\cdot)$  is the hypergeometric function.

*Proof:* The proof is provided in Appendix A. ■

2) *Cell-edge/weak user:* The received signal at the DL cell-edge/weak user (user 2) can be expressed as

$$y_{u_{2d}} = \sqrt{P_b l_{b,r}^{-m} l_{r,u_{2d}}^{-m}} \mathbf{g}_{r,u_{2d}} \Theta_r \mathbf{g}_{b,r} \sum_{i=1}^2 \sqrt{\alpha_i} x_{u_{id}} + I_{u_{2d}} + n_{u_{2d}}, \quad (8)$$

where  $n_{u_{2d}}$  is the AWGN at the user,  $n_{u_{2d}} \sim CN(0, \sigma_{u_{2d}}^2)$  and  $I_{u_{2d}}$  is the interference caused by the UL users and given by

$$I_{u_{2d}} = \underbrace{\sqrt{p_{u_{1u}} l_{r,u_{2d}}^{-m} l_{r,u_{1u}}^{-m}} \mathbf{g}_{r,u_{2d}} \Theta_r \mathbf{g}_{r,u_{1u}} x_{u_{1u}}}_{\text{interference from cell-center user}} + \underbrace{\sqrt{p_{u_{2u}} l_{r,u_{2d}}^{-m} l_{r,u_{2u}}^{-m}} \mathbf{g}_{r,u_{2d}} \Theta_r \mathbf{g}_{r,u_{2u}} x_{u_{2u}}}_{\text{interference from cell edge user}}.$$

Thus the SINR at the DL cell-edge user can be written as

$$\gamma_{u_{2d}} = \frac{P_{b_2} A_{u_{2d}}}{P_{b_1} A_{u_{2d}} + p_{u_{1u}} C_{u_{2d}} + p_{u_{2u}} D_{u_{2d}} + \sigma_{u_{2d}}^2}, \quad (9)$$

where  $A_{u_{2d}} = l_{b,r}^{-m} l_{r,u_{2d}}^{-m} |\mathbf{g}_{r,u_{2d}} \Theta_r \mathbf{g}_{b,r}|^2$ ,  $C_{u_{2d}} = l_{r,u_{2d}}^{-m} l_{r,u_{1u}}^{-m} |\mathbf{g}_{r,u_{2d}} \Theta_r \mathbf{g}_{r,u_{1u}}|^2$ ,  
 $D_{u_{2u}} = l_{r,u_{2d}}^{-m} l_{r,u_{2u}}^{-m} |\mathbf{g}_{r,u_{2d}} \Theta_r \mathbf{g}_{r,u_{2u}}|^2$ .

**Theorem 2.** *The ergodic DL rate of the cell-edge user in passive STAR-RIS-aided FD communication systems under Rician fading channels can be calculated by*

$$\mathcal{E} [R_{u_{2d}}] \approx \log_2 (1 +$$

$$\frac{P_{b_2} x_{1u_{2d}}}{P_{b_1} x_{1u_{2d}} + p_{u_{1u}} y_{1u_{2d}} + p_{u_{2u}} y_{2u_{2d}} + \sigma_{u_{2d}}^2}) \quad (10)$$

where

$$x_{1u_{2d}} = l_{b,r}^{-m} \left( \frac{2(1+R_r)^{-m} (-1+R_r^2+mR_r(1+R_r)+(1+R_r)^m)}{(m-2)(m-1)R_r^2} \right) (\varpi_{b,r}^{r,u_{2d}} \xi_4 + \hat{\varpi}_{b,r}^{r,u_{2d}}) \quad (11)$$

$$y_{1u_{2d}} = \frac{2(1+R_r)^{-m} (-1+R_r^2+mR_r(1+R_r)+(1+R_r)^m) \Upsilon(\varpi_{r,u_{1u}}^{r,u_{2d}} \xi_5 + \hat{\varpi}_{r,u_{1u}}^{r,u_{2d}})}{(m-2)(m-1)R_r^2} \quad (12)$$

$$y_{2u_{2d}} = \left( \frac{2(1+R_r)^{-m} (-1+R_r^2+mR_r(1+R_r)+(1+R_r)^m)}{(m-2)(m-1)R_r^2} \right)^2 (\varpi_{r,u_{2u}}^{r,u_{2d}} \xi_6 + \hat{\varpi}_{r,u_{2u}}^{r,u_{2d}}) \quad (13)$$

*Proof:* The proof is provided in Appendix B. ■

## B. UL

In the UL mode, the received signal at the BS can be written as

$$y_b = \sqrt{p_{u_{1u}}} x_{u_{1u}} \left( \sqrt{l_{b,u_{1u}}^{-m}} h_{b,u_{1u}} + \sqrt{l_{b,r}^{-m} l_{r,u_{1u}}^{-m}} \mathbf{g}_{b,r} \Theta_t \mathbf{g}_{r,u_{1u}} \right) +$$

$$\sqrt{p_{u_{2u}} l_{b,r}^{-m} l_{r,u_{2u}}^{-m}} \mathbf{g}_{b,r} \Theta_t \mathbf{g}_{r,u_{2u}} x_{u_{2u}} + I_b + n_b \quad (14)$$

where  $n_b$  is the AWGN at the BS,  $n_b \sim CN(0, \sigma_b^2)$  and  $I_b$  is the interference term

$$I_b = \underbrace{\sqrt{P_b} h_{b,b} s}_{\text{self interference}} + \underbrace{\sqrt{P_b l_{b,r}^{-m} l_{r,b}^{-m}} \mathbf{g}_{b,r} \Theta_t \mathbf{g}_{b,r} s}_{\text{reflection of the downlink signal}}.$$

Several self-interference suppression (SIS) methods have been proposed in the literature to eliminate the self-interference at the BS [31], [32]. Applying these interference cancellation techniques can reduce the self-interference to the background noise level. In this work, similar to [31], [32], the residual self-interference is assumed to be zero-mean Gaussian distributed with variance  $V$ ,  $\tilde{s} \sim CN(0, V)$ <sup>1</sup>. Thus, the interference term  $I_b$  can be rewritten as

$$I_b = \underbrace{\tilde{s}}_{\text{residual self interference}} + \underbrace{\sqrt{P_b l_{b,r}^{-m} l_{r,b}^{-m}} \mathbf{g}_{b,r}^H \Theta_t \mathbf{g}_{b,r} s}_{\text{reflection of the downlink signal}}.$$

Based on the experimental results, the variance of the residual self interference can be considered mathematically as  $V = \beta P_b^\lambda$ , where the constants  $\beta$  and  $\lambda$  ( $0 \leq \lambda \leq 1$ ) reflect the efficiency of the cancellation technique.

1) *Cell-Center user*: Now, we can write the SINR at the BS to detect the UL cell-center/strong user message as

$$\gamma_{u_{1u}} = \frac{p_{u_{1u}} A_{u_{1u}}}{p_{u_{2u}} B_{u_{1u}} + P_b C_{u_{1u}} + |\tilde{s}|^2 + \sigma_b^2}, \quad (15)$$

where

$$A_{u_{1u}} = \left| \sqrt{l_{b,u_{1u}}^{-m}} h_{b,u_{1u}} + \sqrt{l_{b,r}^{-m} l_{r,u_{1u}}^{-m}} \mathbf{g}_{b,r} \Theta_t \mathbf{g}_{r,u_{1u}} \right|^2, \\ B_{u_{1u}} = l_{b,r}^{-m} l_{r,u_{2u}}^{-m} |\mathbf{g}_{b,r} \Theta_t \mathbf{g}_{r,u_{2u}}|^2, \quad C_{u_{1u}} = l_{b,r}^{-m} l_{r,b}^{-m} |\mathbf{g}_{b,r} \Theta_t \mathbf{g}_{b,r}^H|^2.$$

<sup>1</sup>According to the central limit theorem, this Gaussian assumption might occur in practice due to the several sources of imperfection cancellation stages. Otherwise, the Gaussian assumption can represent the worst-case or lower-bound of the achievable data rate.

**Theorem 3.** *The ergodic UL rate of the cell-center user in passive RIS-aided FD communication systems under Rician fading channels can be calculated by*

$$\mathcal{E} [R_{u_{1u}}] \approx \log_2 \left( 1 + \frac{p_{u_{1u}} x_{1u_{1u}}}{p_{u_{2u}} y_{1u_{1u}} + P_b y_{2u_{1u}} + V + \sigma_b^2} \right), \quad (16)$$

where

$$x_{1u_{1u}} = \frac{2(1+R)^{-m}(-1+R^2+mR(1+R)+(1+R)^m)}{(m-2)(m-1)R^2} + l_{b,r}^{-m} \Upsilon(\varpi_{b,r}^{r,u_{1u}} \xi_7 + \hat{\varpi}_{b,r}^{r,u_{1u}}) \quad (17)$$

$$y_{1u_{1u}} = l_{b,r}^{-m} \frac{2(1+R_r)^{-m}(-1+R_r^2+mR_r(1+R_r)+(1+R_r)^m)(\varpi_{b,r}^{r,u_{2u}} \xi_8 + \hat{\varpi}_{b,r}^{r,u_{2u}})}{(m-2)(m-1)R_r^2} \quad (18)$$

$$y_{2u_{1u}} = l_{b,r}^{-m} l_{b,r}^{-m} \left( \left( \frac{\kappa_{b,r}}{\kappa_{b,r}+1} \right)^2 \xi_9 + 2 \frac{\kappa_{b,r}}{\kappa_{b,r}+1} \frac{1}{\kappa_{b,r}+1} \sum_{n=1}^N |\rho_n^k|^2 + \right.$$

$$\left. \left( \frac{1}{\kappa_{b,r}+1} \right)^2 \left( 2 \sum_{n=1}^N |\rho_n^k|^2 + \sum_{n_1=1}^N \sum_{n_2 \neq n_1}^N (\rho_{n_1}^k e^{j\phi_{n_1}^k}) (\rho_{n_2}^k e^{j\phi_{n_2}^k})^H \right) + 2 \frac{\kappa_{b,r}}{\kappa_{b,r}+1} \frac{1}{\kappa_{b,r}+1} \left( \zeta \sum_{n=1}^N \rho_n^k e^{j\phi_n^k} \right) \right) \quad (19)$$

*Proof:* The proof is provided in Appendix C ■

2) *Cell-edge user:* The SINR at the BS to detect the UL cell-edge/weak user message can be written as

$$\gamma_{u_{2u}} = \frac{p_{u_{2u}} A_{u_{2u}}}{\Xi p_{u_{1u}} B_{u_{2u}} + P_b C_{u_{2u}} + |\tilde{s}|^2 + \sigma_b^2}, \quad (20)$$

where  $A_{u_{2u}} = l_{b,r}^{-m} l_{r,u_{2u}}^{-m} |\mathbf{g}_{b,r} \Theta_t \mathbf{g}_{r,u_{2u}}|^2$ ,

$B_{u_{2u}} =$

$$\left| \sqrt{l_{b,u_{1u}}^{-m}} h_{b,u_{1u}} + \sqrt{l_{b,r}^{-m} l_{r,u_{1u}}^{-m}} \mathbf{g}_{b,r} \Theta_t \mathbf{g}_{r,u_{1u}} \right|^2,$$

$$C_{u_{2u}} = l_{b,r}^{-m} l_{b,r}^{-m} \left| \mathbf{g}_{b,r} \Theta_t \mathbf{g}_{b,r}^H \right|^2.$$

**Theorem 4.** *The ergodic UL rate of the cell-edge user in passive RIS-aided FD communication systems under Rician fading channels can be calculated by*

$$\mathcal{E} [R_{u_{2u}}] \approx \log_2 \left( 1 + \frac{p_{u_{2u}} x_{1u_{2u}}}{\Xi p_{u_{1u}} y_{1u_{2u}} + P_b y_{2u_{2u}} + V + \sigma_b^2} \right) \quad (21)$$

where  $x_{1u_{2u}} = y_{1u_{1u}}$ ,  $y_{1u_{2u}} = x_{1u_{1u}}$ ,  $y_{2u_{2u}} = y_{2u_{1u}}$ .

**Remark.** All the ergodic rate expressions in this work are presented in closed form. Thus, the impact of the system parameters on the total achievable data rates can be observed, and the optimal design can be attained. Simpler expressions can be easily obtained by relaxing the practical assumptions, such as perfect SIC, ignoring the signals reflected from the RIS to the cell center users, assuming the users are located in fixed locations, and perfect self interference cancellation. Accordingly, the ergodic rate expressions presented in Theorems 1-4 can be simplified into,

$$\mathcal{E} [R_{u_{1d}}] \approx \log_2 \left( 1 + \frac{P_{b_1} l_{b,u_{1d}}^{-m}}{p_{u_{1u}} l_{u_{1d},u_{1u}}^{-m} + y_{u_{1d}} + \sigma_{u_{1d}}^2} \right) \quad (22)$$

$$\mathcal{E} [R_{u_{2d}}] \approx \log_2 \left( 1 + \frac{P_{b_2} x_{u_{2d}}}{P_{b_1} x_{u_{2d}} + y_{2u_{2d}} + y_{3u_{2d}} + \sigma_{u_{2d}}^2} \right) \quad (23)$$

$$\mathcal{E} [R_{u_{1u}}] \approx \log_2 \left( 1 + \frac{p_{u_{1u}} l_{b,u_{1u}}^{-m}}{y_{2u_{1u}} + \sigma_b^2} \right) \quad (24)$$

$$\mathcal{E} [R_{u_{2u}}] \approx \log_2 \left( 1 + \frac{x_{u_{2u}}}{\sigma_b^2 (\kappa_{r,u_{2u}} + 1) (\kappa_{b,r} + 1)} \right) \quad (25)$$

where

$$\begin{aligned} y_{u_{1d}} &= p_{u_{2u}} l_{r,u_{2u}}^{-m} l_{r,u_{1d}}^{-m} (\varpi_{r,u_{2u}}^r \xi_3 + \hat{\varpi}_{r,u_{2u}}^r), \\ x_{u_{2d}} &= l_{b,r}^{-m} l_{r,u_{2d}}^{-m} (\varpi_{b,r}^r \xi_4 + \hat{\varpi}_{b,r}^r), \\ y_{2u_{2d}} &= p_{u_{1u}} l_{r,u_{2d}}^{-m} l_{r,u_{1u}}^{-m} (\varpi_{u_{1u},r}^r \xi_5 + \hat{\varpi}_{u_{1u},r}^r), \\ y_{3u_{2d}} &= p_{u_{2u}} l_{r,u_{2d}}^{-m} l_{r,u_{2u}}^{-m} (\varpi_{r,u_{2u}}^r \xi_6 + \hat{\varpi}_{r,u_{2u}}^r), \\ y_{2u_{1u}} &= p_{u_{2u}} l_{b,r}^{-m} l_{r,u_{2u}}^{-m} (\varpi_{b,r}^r \xi_8 + \hat{\varpi}_{b,r}^r), \\ x_{u_{2u}} &= p_{u_{2u}} l_{b,r}^{-m} l_{r,u_{2u}}^{-m} \kappa_{r,u_{2u}} \kappa_{b,r} \xi_8 + \\ & p_{u_{2u}} l_{b,r}^{-m} l_{r,u_{2u}}^{-m} \sum_{n=1}^N |\rho_n^k|^2 (\kappa_{r,u_{2u}} + \kappa_{b,r} + 1). \end{aligned}$$

#### IV. BIDIRECTIONAL COMMUNICATION

Besides other applications, the above results can be used to analyze the performance of STAR-RIS networks with bidirectional communication tasks, which can be interpreted as bidirectional relaying where the BS plays the role of the relay node [33]. In this context, we will focus on the most difficult scenario, when the UL cell-center user communicates with the DL cell-edge, and the UL cell-edge user communicates with the DL cell-center user through the FD-BS. Particularly, in each time slot the UL users transmit their data to the FD-BS, and the BS broadcasts the data to the DL users using NOMA pairing scheme.

##### A. UL Cell-edge user to DL Cell-center user

The received signal at the DL cell-center user can be expressed by

$$\begin{aligned} y_{u_{1d}} &= \sqrt{p_{u_{2u}} l_{r,u_{2u}}^{-m} l_{r,u_{1d}}^{-m}} \mathbf{g}_{r,u_{1d}} \Theta_t \mathbf{g}_{r,u_{2u}} x_{u_{2u}} + \\ & \sum_{i=1}^2 \sqrt{P_{b_i}} \hat{x}_{u_{iu}} \left( \sqrt{l_{b,u_{1d}}^{-m}} h_{b,u_{1d}} + \right. \\ & \left. \sqrt{l_{b,r}^{-m} l_{r,u_{1d}}^{-m}} \mathbf{g}_{r,u_{1d}} \Theta_t \mathbf{g}_{b,r} \right) \end{aligned}$$

$$+I_{u_{1d}} + n_{u_{1d}}, \quad (26)$$

where the interference term is given by

$I_{u_{1d}} = \sqrt{p_{u_{1u}}} x_{u_{1u}} \left( \sqrt{l_{u_{1d},u_{1u}}^{-m}} h_{u_{1d},u_{1u}} + \sqrt{l_{r,u_{1u}}^{-m} l_{r,u_{1d}}^{-m}} \mathbf{g}_{r,u_{1d}} \Theta_t \mathbf{g}_{r,u_{1u}} \right)$ . Recall that  $\hat{x}_{u_{2u}} = x_{u_{2u}} (\bar{i} - \hat{\tau})$ , where  $\bar{i}$  denotes the  $\bar{i}$ th time slot and  $\hat{\tau}$  is the decoding time of the message at the BS. Assuming that the processing delay caused by the detection process at the BS is small compared to the duration of one channel use, i.e.,  $\hat{\tau} \leq \hat{t}_{i+1} - \hat{t}_i$ , where  $\hat{t}_{i+1}$  and  $\hat{t}_i$  denote the  $(\bar{i}+1)$ th and the  $\bar{i}$ th time slots, respectively. Thus, the cell-center user receives the message  $x_{u_{2u}}$  from the BS and the cell-edge user at approximately the same channel use. Hence, the user can successfully combine the signal  $\hat{x}_{u_{2u}}$  transmitted from the BS and the signal  $x_{u_{2u}}$  from the UL cell-edge user by a proper diversity-combining technique such as maximum ratio combining (MRC) [34]. Consequently, the achievable rate of the DL cell-center user can be expressed by

$$R_{uc} = \log_2 \left( 1 + \frac{p_{u_{2u}} a_{u_{1d}}}{p_{u_{1u}} C_{u_{1d}} + \sigma_{u_{1d}}^2} + \frac{P_{b_1} A_{u_{1d}}}{\Xi P_{b_2} A_{u_{1d}} + p_{u_{1u}} C_{u_{1d}} + \sigma_{u_{1d}}^2} \right), \quad (27)$$

where  $a_{u_{1d}} = l_{r,u_{2u}}^{-m} l_{r,u_{1d}}^{-m} |\mathbf{g}_{r,u_{1d}} \Theta_t \mathbf{g}_{r,u_{2u}}|^2$ .

**Theorem 5.** *The ergodic rate of the DL cell-center user in passive STAR-RIS-aided FD bidirectional communication under Rician fading channels can be calculated by*

$$\bar{R}_c = \min(\bar{R}_{u_{2u}}, \bar{R}_{uc}) \quad (28)$$

where

$$\bar{R}_{uc} = \log_2 \left( 1 + \frac{p_{u_{2u}} y_{2u_{1d}}}{p_{u_{1u}} y_{1u_{1d}} + \sigma_{u_{1d}}^2} \right)$$

$$+ \frac{P_{b_1} x_{1u_{1d}}}{\Xi P_{b_2} x_{1u_{1d}} + p_{u_{1u}} y_{1u_{1d}} + \sigma_{u_{1d}}^2} \Bigg), \quad (29)$$

and  $\bar{R}_{u_{2u}} = \mathcal{E} [R_{u_{2u}}]$  is given in (21),  $x_{1u_{1d}}, y_{1u_{1d}}, y_{2u_{1d}}$  are defined in (5)-(7).

*Proof:* The proof is based on the analysis in Appendix A. ■

### B. UL Cell-center user to DL Cell-edge user

The received signal at the cell edge user is given by

$$y_{u_{2d}} = \sqrt{p_{u_{1u}} l_{r,u_{2d}}^{-m} l_{r,u_{1u}}^{-m}} \mathbf{g}_{r,u_{2d}} \Theta_r \mathbf{g}_{r,u_{1u}} x_{u_{1u}} \\ + \sqrt{P_b l_{b,r}^{-m} l_{r,u_{2d}}^{-m}} \mathbf{g}_{r,u_{2d}} \Theta_r \mathbf{g}_{b,r} \sum_{i=1}^2 \sqrt{\alpha_i} \hat{x}_{u_{iu}} + I_{u_{2d}} + n_{u_{2d}}, \quad (30)$$

where  $I_{u_{2d}} = \sqrt{p_{u_{2u}} l_{r,u_{2d}}^{-m} l_{r,u_{2u}}^{-m}} \mathbf{g}_{r,u_{2d}} \Theta_r \mathbf{g}_{r,u_{2u}} x_{u_{2u}}$ . Similarly, the achievable rate of the DL cell edge user can be expressed by

$$R_{u_e} = \log_2 \left( 1 + \frac{p_{u_{1u}} a_{u_{2d}}}{D_{u_{2d}} + \sigma_{u_{2d}}^2} \right. \\ \left. + \frac{P_{b_2} A_{u_{2d}}}{P_{b_1} A_{u_{2d}} + p_{u_{2u}} D_{u_{2d}} + \sigma_{u_{2d}}^2} \right), \quad (31)$$

where  $a_{u_{2d}} = l_{r,u_{2d}}^{-m} l_{r,u_{1u}}^{-m} |\mathbf{g}_{r,u_{2d}} \Theta_r \mathbf{g}_{r,u_{1u}}|^2$ .

**Theorem 6.** *The ergodic rate of the DL cell-edge user in passive STAR-RIS-aided FD bidirectional communication under Rician fading channels can be calculated by*

$$\bar{R}_e = \min (\bar{R}_{u_{1u}}, \bar{R}_{u_e}) \quad (32)$$

where



$$\begin{aligned} \bar{R}_{u_e} \approx \log_2 \left( 1 + \frac{p_{u_{1u}} y_{1u_{2d}}}{p_{u_{2u}} y_{2u_{2d}} + \sigma_{u_{2d}}^2} \right. \\ \left. + \frac{P_{b_2} x_{1u_{2d}}}{P_{b_1} x_{1u_{2d}} + p_{u_{2u}} y_{2u_{2d}} + \sigma_{u_{2d}}^2} \right), \end{aligned} \quad (33)$$

and  $\bar{R}_{u_{1u}} = \mathcal{E} [R_{u_{1u}}]$  is given in (16),  $x_{1u_{2d}}, y_{1u_{2d}}, y_{2u_{2d}}$  are defined in (11)-(13).

*Proof:* The proof is based on the analysis in Appendix B. ■

## V. SYSTEMS DESIGN

As we can notice from the previous sections, the ergodic rates are function of the STAR-RIS amplitudes and phase shifts and the UL and DL transmit powers. Therefore, these parameters can be optimized to maximize the total weighted sum rate. Accordingly, the optimization problem for both scenarios can be formulated as

$$\begin{aligned} & \max_{\rho, \theta, \mathbf{p}} f(\theta, \rho, \mathbf{p}) \\ (C.1) \quad & \text{s.t. } \sum_{i=1}^2 p_{u_{iu}} + P_{b_i} \leq P_t, p_{u_{iu}} \geq 0, P_{b_i} \geq 0 \\ (C.2) \quad & R_{u_{1d} \rightarrow u_{2d}} \geq R_{u_{2d}} \\ (C.3) \quad & R_{u_{2d}} \geq R_{d_{th}}, R_{u_{2u}} \geq R_{u_{th}} \\ (C.4) \quad & (\rho_n^r) + (\rho_n^t) = 1, \forall n \in N \\ (C.5) \quad & \rho_n^k \geq 0, |\theta_n^k| = 1, \forall n \in N \end{aligned} \quad (34)$$

where  $f(\theta, \rho, \mathbf{p}) = \sum_{i=1}^2 (\omega_{id} \bar{R}_{u_{id}} + \omega_{iu} \bar{R}_{u_{iu}})$ , and  $f(\theta, \rho, \mathbf{p}) = \omega_{u_c} \bar{R}_{u_c} + \omega_{u_e} \bar{R}_{u_e}$  for the bidirectional communication scenario,  $\theta = [\theta^t, \theta^r]$ ,  $\rho = [\rho^t, \rho^r]$ ,  $\mathbf{p} = [p_{u_1}, p_{u_2}, P_{b_1}, P_{b_2}]^T$ , and  $P_t$  is the total transmission power  $P_t = \tau P_b + (1 - \tau) P_u$ ,  $P_u = p_{u_1} + p_{u_2}$ ,  $0 < \tau \leq 1$ ,  $\omega_i$  are the weighting factors, which signify the priority assigned to each user. The first constraint (C.1) upper bounds the network transmit power, where the transmit powers are larger than zero, while the second

constraint (C.2) provides the fundamental condition for the implementation of SIC<sup>2</sup>. The third constraint (C.3) is required to provide a fair power allocation scheme for the cell-edge users. The last two constraints (C.4) and (C.5) for the amplitude and phase shift on each STAR-RIS element. It is extremely difficult to find a solution for the problem due to its non convexity in nature. However, the main problem can be divided into two sub-problems: 1) Fix  $\mathbf{p}$  and optimize  $\rho, \theta$  to maximize the sum rate, 2) Fix  $\rho, \theta$  and reformulate the problem to optimize  $\mathbf{p}$ .

#### A. Simultaneous Amplitudes And Phase-Shifts Optimization

For a given power transmission, the main problem can be simplified into a sub-problem to maximize the sum rate with the amplitudes and phase-shifts as follows

$$\begin{aligned} & \max_{\rho, \theta} f(\theta, \rho) \\ \text{s.t } & (\rho_n^r) + (\rho_n^t) = 1, \forall n \in N, \\ & \rho_n^k \geq 0, |\theta_n^k| = 1, \forall n \in N. \end{aligned} \quad (35)$$

The two optimization variables in (35) with the non-convexity make the problem hard to solve. However, the projected gradient ascent method (PGAM), can be applied to obtain the optimal amplitudes and the phase shifts simultaneously. To apply the PGAM, we denote,  $\Phi = \{\theta^t \in \mathbb{C}^{N \times 1}, \theta^r \in \mathbb{C}^{N \times 1} \mid |\theta^r| = |\theta^t| = 1\}$ , and  $Q = \{\rho^t, \rho^r \in \mathbb{C}^{N \times 1} \mid (\rho_i^t) + (\rho_i^r) = 1, \rho_i^k \geq 0\}$ .

Then, we compute the gradients of  $f(\theta, \rho)$  with respect to  $\theta$ ,  $\nabla_{\theta} f(\theta^i, \rho^i)$ , and  $\rho$ ,  $\nabla_{\rho} f(\theta^i, \rho^i)$ . Next the RIS phases and amplitudes are updated at each iteration using the following expressions,  $\theta^{i+1} = (\theta^i + \mu_i \nabla_{\theta} f(\theta^i, \rho^i))$  and  $\rho^{i+1} = (\rho^i + \alpha \mu_i \nabla_{\rho} f(\theta^i, \rho^i))$ , where  $\mu_i$  and  $\alpha \mu_i$  correspond to the step sizes. Then we project them onto  $\Phi$  and  $Q$ . The overall algorithm is summarized in Algorithm 1.

<sup>2</sup>In UL the BS is the receiver, thus it can achieve SIC in any users order.

---

**Algorithm 1** Optimization Algorithm.
 

---

Input: Given a tolerance  $\epsilon > 0$  and the maximum number of iterations  $L$ . Initialize  $\rho^{(0)}$ , and  $\theta^{(0)}$ .  
 . Set step size  $\mu = 0.5$ .  
 for  $i = 0$  to  $L$  do  
 Evaluate:  $f(\theta^{(i)}, \rho^{(i)})$ , then  $\nabla_{\theta} f(\theta^{(i)}, \rho^{(i)})$ , and  $\nabla_{\rho} f(\theta^{(i)}, \rho^{(i)})$   
 Update:  $\theta^{i+1} = (\theta^i + \mu \nabla_{\theta} f(\theta^i, \rho^i))$  and  $\rho^{i+1} = (\rho^i + \alpha \mu \nabla_{\rho} f(\theta^i, \rho^i))$   
 Evaluate:  $f(\theta^{(i+1)}, \rho^{(i+1)})$   
 Until Convergence:  $f(\theta^{(i+1)}, \rho^{(i+1)}) - f(\theta^{(i)}, \rho^{(i)}) < \epsilon$ .

---

1) *Sub-optimal Design*: The phase shifts and amplitude coefficients can be obtained based on the ergodic rate expressions and the cell-edge users channels as follows. The cell-edge users have higher preference in the STAR-RIS design, thus as an efficient simple design, the phase shifts of the elements,  $\theta^r$  and  $\theta^t$ , can be aligned to the cell-edge users channels. Hence, the phase shifts can be presented in terms of the BS-RIS and RIS-user channels as,  $\phi_n^k = -2\pi \frac{d}{\lambda} (x_n t_{b,u_{2k}} + y_n l_{b,u_{2k}})$ ,  $k \in \{t, r\}$  where  $t_{u_{2k}} = \sin \varphi_{b,r}^a \sin \varphi_{b,r}^e - \sin \varphi_{r,u_{2k}}^a \sin \varphi_{r,u_{2k}}^e$ , and  $l_{u_{2k}} = \cos \varphi_{b,r}^e - \cos \varphi_{r,u_{2k}}^e$ , while  $\varphi_{x,y}^a, \varphi_{x,y}^e$  denote the azimuth and elevation angles of arrival (AoA) from node  $x$  to node  $y$ ,  $\lambda$  is the wavelength,  $d$  is the elements spacing, and  $x_n = (n-1) \bmod \sqrt{N}$ ,  $y_n = \frac{n-1}{\sqrt{N}}$ . Then, the amplitude coefficients  $\rho_n^r$  and  $\rho_n^t$  can be calculated from the ergodic rate expressions in Theorems 2 and 4 according to the required data rates at cell-edge users.

For the bidirectional communication scenario, the total SINR is a combination of two parts,  $\gamma = \gamma_1 + \gamma_2$ , where  $\gamma_1$  is the SINR due to user-RIS-user link, and  $\gamma_2$  is the SINR for BS-RIS-user link. As a sub-optimal design, the STAR-RIS can be designed based on the maximum SINR, i.e.,  $\max(\gamma_1, \gamma_2)$ . In case  $\gamma_1$  is the maximum SINR the phase shifts can be aligned to the user-RIS-user channels as,  $\phi_n^k = -2\pi \frac{d}{\lambda} (x_n t_{u_{1\bar{k}},u_{2k}} + y_n l_{u_{1\bar{k}},u_{2k}})$ , and in case  $\gamma_2$  is the maximum SINR, the phase shifts can be aligned to the BS-RIS-user channels as,  $\phi_n^k = -2\pi \frac{d}{\lambda} (x_n t_{b,u_{2k}} + y_n l_{b,u_{2k}})$ .

### B. Power Allocation

The optimal values of the transmission powers can be obtained by reformulating the problem in (35) as

$$\begin{aligned}
& \max_{\mathbf{p}} \sum_{i=1}^2 f(\mathbf{p}) \\
\text{s.t. } & \sum_{i=1}^2 p_{u_{iu}} + P_{b_i} \leq P_t, p_{u_{iu}} \geq 0, P_{b_i} \geq 0 \\
& \bar{R}_{u_{1d} \rightarrow u_{2d}} \geq \bar{R}_{u_{2d}} \\
& \bar{R}_{u_{2d}} \geq R_{d_{th}}, \bar{R}_{u_{2u}} \geq R_{u_{th}}.
\end{aligned} \tag{36}$$

This problem can be solved optimally by applying several schemes such as monotonic optimization, and block coordinate descent (BCD) iterative algorithms as explained in [35], [36], the details are omitted here due to paucity of space. Additionally in this work, based on the derived ergodic rate expressions we present a simple and efficient power allocation scheme.

1) *Sub-optimal Design:* The DL and UL power transmission can be obtained by solving simple equations as follows. The transmission power for the cell-edge users  $p_{u_{2u}}$  and  $P_{b_2}$  can be obtained by satisfying the last fairness constraint with equality, e.g.,  $\bar{R}_{u_{2d}} = R_{d_{th}}, \bar{R}_{u_{2u}} = R_{u_{th}}$  where  $\bar{R}_{u_{2d}}$  and  $\bar{R}_{u_{2u}}$  are presented in Theorems 2 and 4, respectively. Also,  $P_{b_1}$  can be found by achieving the required SIC condition,  $\bar{R}_{u_{1d} \rightarrow u_{2d}} = R_{d_{th}}$ , and hence  $p_{u_{1u}} = P_t - \left( p_{u_{2u}} + \sum_{i=1}^2 P_{b_i} \right)$ . Considering these equations together, we can find the DL and UL power values as

$$P_{b_1} = P_t \frac{(c_1 - c_2)}{(b_2 - b_1)} - \frac{(q_1 - q_2)}{(b_2 - b_1)} \tag{37}$$

$$P_{b_2} = P_t \left( b_1 \frac{(c_1 - c_2)}{(b_2 - b_1)} + b_2 \right) - b_1 \frac{(q_1 - q_2)}{(b_2 - b_1)} - q_2 \tag{38}$$

$$\begin{aligned}
p_{u_{2u}} = P_t & \left( \frac{(c_1 - c_2)}{(b_2 - b_1)} R_{u_{th}} \frac{y_{2u_{2u}}}{x_{1u_{2u}}} + \right. \\
& \left. \left( b_2 \frac{(c_1 - c_2)}{(b_2 - b_1)} + c_2 \right) R_{u_{th}} \frac{y_{2u_{2u}}}{x_{1u_{2u}}} \right) + \hat{c}
\end{aligned} \tag{39}$$

where  $b_i = \frac{a_i - e_i R_{d_{th}} - e_i R_{d_{th}} R_{u_{th}} \frac{y_{2u_{2u}}}{x_{1u_{2u}}}}{1 + e_i R_{d_{th}} + e_i R_{d_{th}} R_{u_{th}} \frac{y_{2u_{2u}}}{x_{1u_{2u}}}}$ ,  $c_i = \frac{e_i R_{d_{th}}}{1 + e_i R_{d_{th}} + e_i R_{d_{th}} R_{u_{th}} \frac{y_{2u_{2u}}}{x_{1u_{2u}}}}$ ,  $q_i = \frac{w_i}{1 + e_i R_{d_{th}} + e_i R_{d_{th}} R_{u_{th}} \frac{y_{2u_{2u}}}{x_{1u_{2u}}}}$ ,

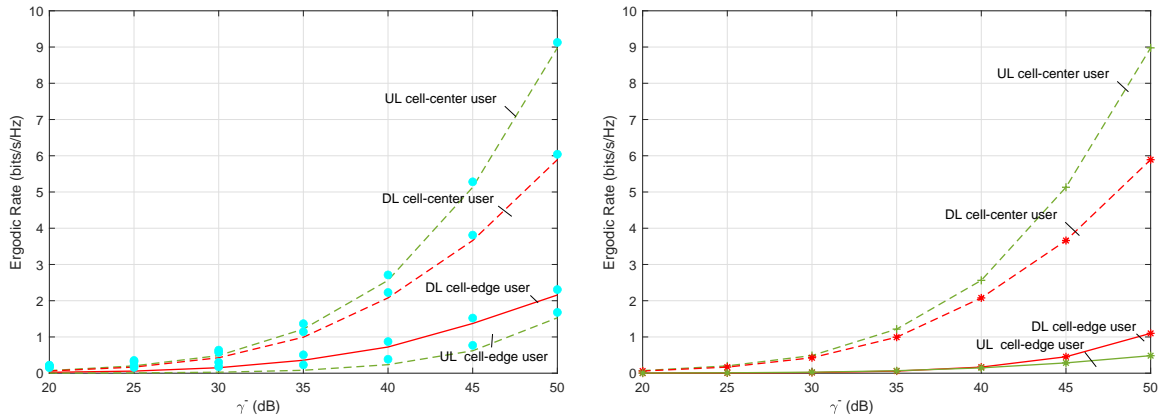
$$\begin{aligned}
a_i &= \frac{R_{d_{th}} + R_{u_{th}} R_{d_{th}} \frac{y_{2u_{id}}}{x_{1u_{id}}} \frac{y_{2u_{2u}}}{x_{1u_{2u}}}}{1 - R_{u_{th}} R_{d_{th}} \frac{y_{2u_{id}}}{x_{1u_{id}}} \frac{y_{2u_{2u}}}{x_{1u_{2u}}}}, \quad e_i = \frac{y_{1u_{id}}}{x_{1u_{id}} \left( 1 - R_{u_{th}} R_{d_{th}} \frac{y_{2u_{id}}}{x_{1u_{id}}} \frac{y_{2u_{2u}}}{x_{1u_{2u}}} \right)}, \\
w_i &= a_i R_{d_{th}} R_{u_{th}} \frac{V}{x_{1u_{2u}}} - e_i R_{d_{th}} R_{u_{th}} \frac{\sigma_b^2}{x_{1u_{2u}}} - z_i, \quad z_i = \frac{\eta_i}{1 - R_{u_{th}} R_{d_{th}} \frac{y_{2u_{id}}}{x_{1u_{id}}} \frac{y_{2u_{2u}}}{x_{1u_{2u}}}}, \\
\eta_i &= R_{u_{th}} R_{d_{th}} \frac{y_{2u_{id}}}{x_{1u_{id}}} \frac{V}{x_{1u_{2u}}} + R_{u_{th}} R_{d_{th}} \frac{y_{2u_{id}}}{x_{1u_{id}}} \frac{\sigma_b^2}{x_{1u_{2u}}} + R_{d_{th}} \frac{\sigma_{u_{2d}}^2}{x_{1u_{2d}}} \quad \text{and} \\
\hat{c} &= -\frac{(q_1 - q_2)}{(b_2 - b_1)} R_{u_{th}} \frac{y_{2u_{2u}}}{x_{1u_{2u}}} - b_2 \frac{(q_1 - q_2)}{(b_2 - b_1)} R_{u_{th}} \frac{y_{2u_{2u}}}{x_{1u_{2u}}} - q_2 R_{u_{th}} \frac{y_{2u_{2u}}}{x_{1u_{2u}}} + R_{u_{th}} \frac{V}{x_{1u_{2u}}} + R_{u_{th}} \frac{\sigma_b^2}{x_{1u_{2u}}}.
\end{aligned}$$

*Proof:* The proof is provided in Appendix D. ■

## VI. NUMERICAL RESULTS

In this section, we present simulation and numerical results to validate our analysis, and to examine the effects of different parameters on the overall system performance. The radius of the cell-center region is  $R = 50m$ , while the radius of the cell-edge region is  $R_r = 30m$ . For simplicity, the transmit SNR is defined as  $\bar{\gamma} = \frac{P_t}{\sigma^2}$ , the Rician factors are 3,  $\beta = 0.001$ ,  $\lambda = 0.1$ ,  $\omega = 0.8$  and the path loss exponent is  $m = 2.7$  [37]. Number of RIS elements  $N = 20$ , number of users is  $K_c = K_e = 6$ .

Firstly, in Fig. 2 we illustrate the ergodic rates versus the transmit SNR,  $\bar{\gamma}$ . Fig. 2a shows the achievable rates using optimal phase shifts, while the achievable rates with random phase shifts are presented in Fig. 2b. It is evident from these figures that the analytical and simulation results are in good agreement, which confirms the accuracy of the analysis. It is also clear that the ergodic rates are enhanced with an increase in the transmit SNR for both scenarios. In addition, it can be observed that the ergodic rates of the edge users utilizing the optimal phase shifts are higher than those utilizing random phase shifts. On the other hand, the performance of the cell-center users does not depend essentially on the STAR-RIS phase shifts. It has been also noted that 80% of the total power has been allocated for the DL transmission, while 20% for the UL. This is due to the impact of the interference power at the DL users.



(a) Ergodic rates versus transmit SNR  $\bar{\gamma}$ , with optimal phase shifts. (b) Ergodic rates versus transmit SNR  $\bar{\gamma}$ , with random phase shifts.

Figure 2. Ergodic rates versus transmit SNR,  $\bar{\gamma}$ , for different phase shifts.

To demonstrate the impact of the system impairments on the users performance, in Fig. 3 we plot the ergodic rates versus the transmit SNR,  $\bar{\gamma}$ , for different values of the SIC error factor, and the variance of the residual self interference. Specifically, Fig. 3a depicts the impact of the imperfect SIC on the achievable rates, while Fig. 3b investigates the impact of imperfect self interference suppression, SIS, at the BS. Comparing Fig. 3a and Fig. 2a, it can be noted that the imperfect SIC results in degrading the ergodic rates of the DL cell center user and the UL cell edge user, as their performance rely on the SIC detection scheme. In addition, from Figs. 3b and Fig. 2a we can see that, the performance of the UL users degrade greatly as the variance of the residual self interference rises.

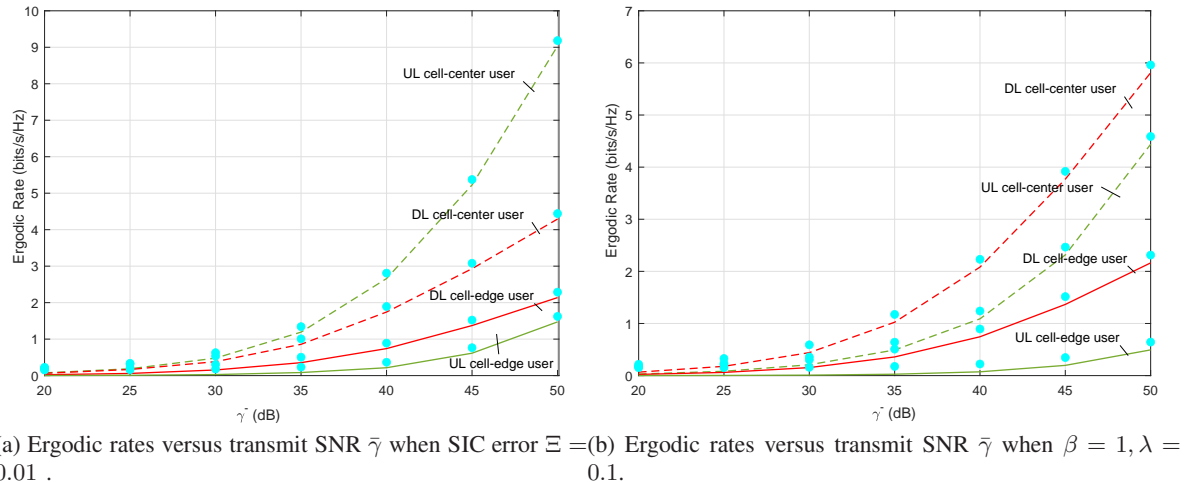
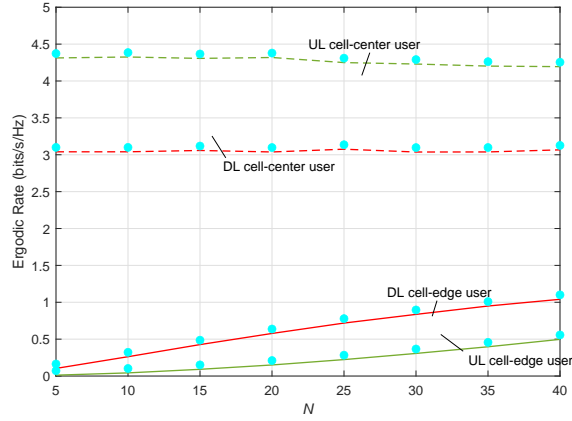
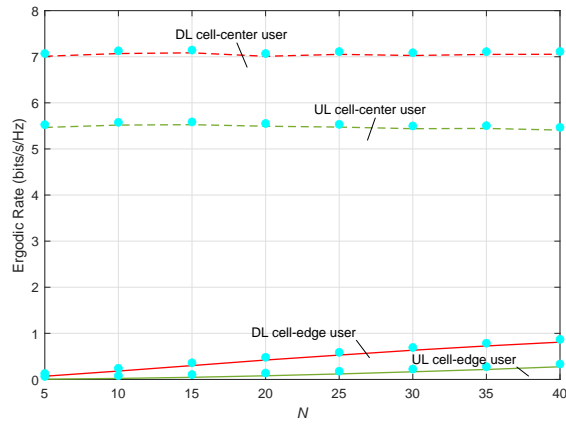


Figure 3. Ergodic rates versus transmit SNR  $\bar{\gamma}$  with SIC error and self interference.

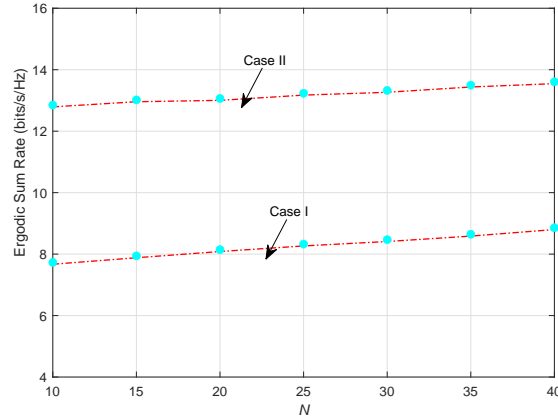
Furthermore, in Fig. 4, we depict the ergodic rates and sum-rates versus number of STAR-RIS elements,  $N$ , for different edge users' target rates, when  $\bar{\gamma} = 40$  dB. Fig 4a represents the high data rate requirement (case I), and Fig 4b represents the low data rate requirement (case II). Firstly, in general, increasing number of the STAR-RIS elements  $N$  enhances the ergodic rates of the edge users, while the performance of the cell center users is dominant by the direct links between the BS and the users, and their achievable rates almost fixed with  $N$ . Having a closer look at these results, one can observe that, when the data rate requirements of the edge users are relatively high as in case I, more power will be allocated to the edge users and less power to the cell-center users and as a result the total sum rate will be relatively low as shown in Fig. 4c. On the other hand, when the data rate requirements of the edge users are relatively low as in case II, more power will be allocated to the cell-center users and this leads to increase the total sum rates as explained in Fig. 4c.



(a) Ergodic rates versus number of STAR-RIS elements  $N$ , case I.



(b) Ergodic rates versus number of STAR-RIS elements  $N$ , case II.



(c) Ergodic sum rates versus number of STAR-RIS elements  $N$ .

Figure 4. Ergodic rates versus number of STAR-RIS elements  $N$  for different system design.

To explain clearly the impact of the power allocation between the UL and DL transmissions on the total sum-rate, in Fig. 5 we plot the ergodic sum-rate versus the power allocation coefficient,  $\tau$ , for two different values of the maximum target rate at the DL edge user 6 bits/s/Hz and 3



bits/s/Hz, when  $P_t = 50$  dBW. Notably and as expected, when the target rate is high (6 bits/s/Hz) more power will be allocated to the DL edge user, and less power allocated to the DL cell center user. As a result, the DL sum rate will be small and the total sum rate will be dominated by the UL sum rate. For instance, when  $\tau = 0$  all power is allocated to the UL transmission and the achievable sum rate is around 25.6 bits/s/Hz, while when  $\tau = 1$  the all power is allocated to the DL transmission and the achievable sum rate is around 20.4 bits/s/Hz, and the optimal  $\tau$  is 0.2. On the other hand, if the target rate at the DL cell edge user is small (3 bits/s/Hz) more power can be allocated to the DL cell center user. Thus, the DL sum rate will be high and the total sum rate will be dominant by both UL and DL. For instance, when  $\tau = 1$  the achievable sum rate is now around 27.3 bits/s/Hz, and the optimal  $\tau$  in this case is around 0.65.

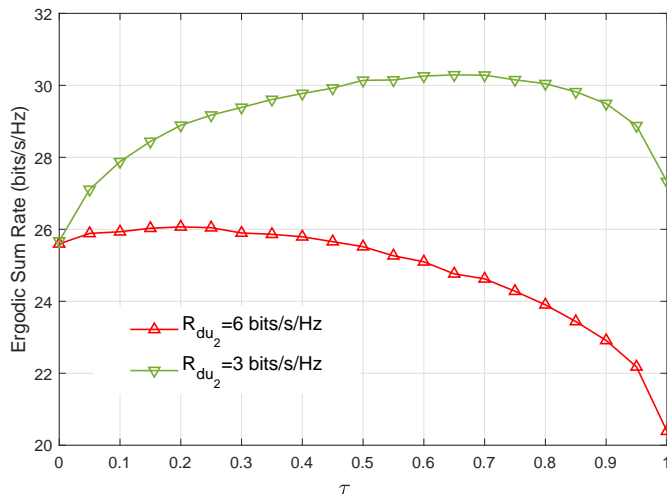


Figure 5. Ergodic sum-rates versus power allocation coefficient.

Moreover, in Fig. 6 we plot the achievable rates of the bidirectional communication scenario against number of the STAR-RIS elements,  $N$ , for the ideal case ( $\Xi = 0$ ,  $V = 0$ ), imperfect SIC ( $\Xi = 0.5$ ) and imperfect SIS ( $V = 1.25$ ) schemes, when  $\bar{\gamma} = 40$  dB. The ergodic rates of the cell-center user and cell-edge user enhance with increasing number of the STAR-RIS units. However, the performance of the cell-center user degrades significantly when the interference cancellation schemes, SIC and SIS, are imperfect/unideal which is not the case for the cell-edge user.

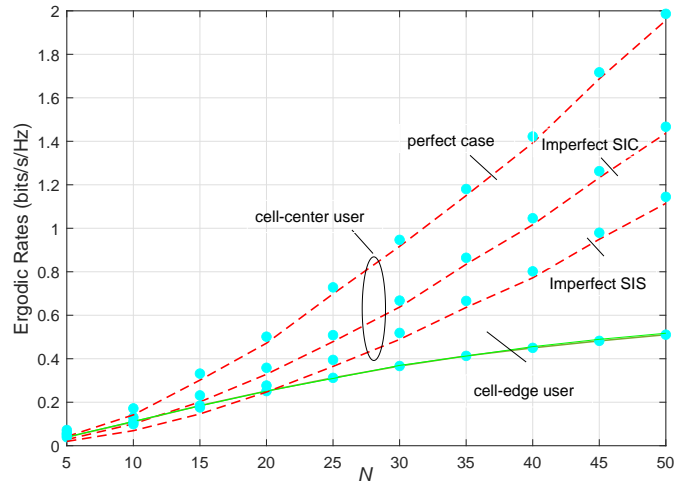


Figure 6. Ergodic rates of the bidirectional communication versus number of STAR-RIS elements  $N$ .

Fig. 7, illustrates the ergodic rates of the bidirectional communication versus the transmit SNR,  $\bar{\gamma}$ . In these results, the required data rate of the edge user is higher than that in Fig. 6, thus high power has been allocated to the edge user at the expense of the cell-center user. As expected, from Fig. 7, the achievable rates of both users can be improved significantly by increasing the transmit SNR.

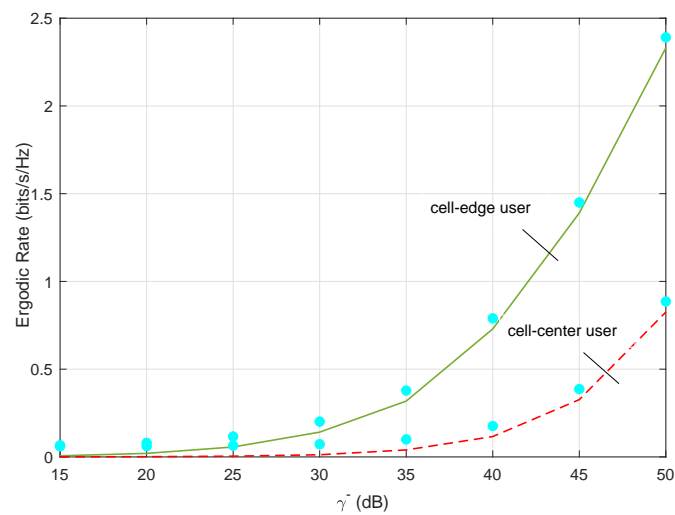


Figure 7. Ergodic rates of the bidirectional communication versus transmit SNR  $\bar{\gamma}$ .

Finally, to investigate the impact of the power allocation on the achievable rates of the bidirectional communication, in Fig. 8 we plot the ergodic rates versus the power allocation coefficient,  $\tau$ , for different cases, case I:  $p_{u_1} = p_{u_2} = 0.5P_u, P_{b_1} = 0.1P_b, P_{b_2} = 0.9P_b$ , case II:  $p_{u_1} = p_{u_2} = 0.5P_u, P_{b_1} = 0.4P_b, P_{b_2} = 0.6P_b$ , and case III:  $p_{u_1} = 0.6, p_{u_2} = 0.4P_u, P_{b_1} = 0.1P_b, P_{b_2} = 0.9P_b$ , when  $P_t = 40$  dBW. From these results, we can notice that the performance of the DL cell-edge user is sensitive to the DL power where increasing the power allocated to the DL cell-edge user at the BS enhances the achievable rate at the user. On the other side, the cell-center user is more sensitive to the UL power and reducing the power allocated to the UL cell-edge user degrades the data rate. Interestingly enough, for each user, there exists an optimal power allocation coefficient. The DL cell-center user reaches the optimal performance with a small value of  $\tau$ , e.g., high power allocated to the UL transmission, while the DL cell-edge user achieves the optimal performance with a high value of  $\tau$ , e.g., high power allocated to the DL transmission.

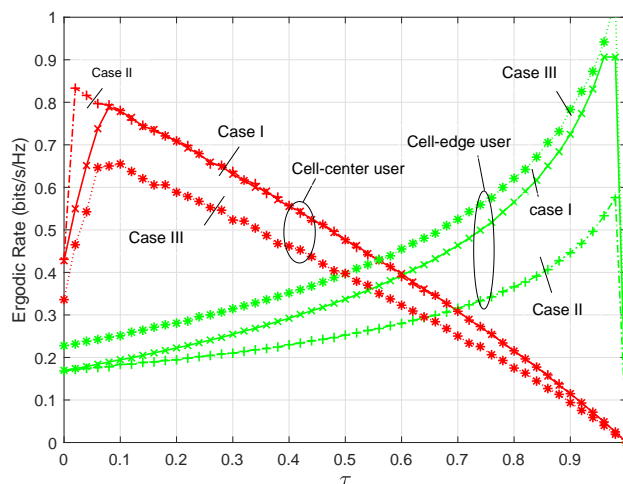


Figure 8. Ergodic rates of the bidirectional communication versus power allocation coefficient.

## VII. CONCLUSIONS

This study investigated a STAR-RIS-assisted FD communication system, with the STAR-RIS deployed at the cell-edge to support cell-edge users. We applied a NOMA pairing scheme and

derived closed-form expressions for the ergodic rates. Additionally, our analysis was extended to encompass bidirectional communication between cell-center and cell-edge users. Furthermore, we formulated and solved an optimization problem aimed at maximizing the achievable sum-rate by determining the optimal STAR-RIS design and power allocation scheme. The results demonstrated that increasing the transmitted SNR enhances achievable rates, and using a large number of STAR-RIS elements improves cell-edge user performance. Additionally, we observed that imperfect SIC degrades the achievable rates of the DL cell-center user and the UL cell-edge user, while imperfect SIS significantly impacts UL user performance.

#### APPENDIX A

By using Jensen inequality, the ergodic rate can be approximated as

$$\mathcal{E} [R_{u_{1d}}] \approx \log_2 \left( 1 + \mathcal{E} \left\{ \frac{P_{b_1} A_{u_{1d}}}{\Xi P_{b_2} A_{u_{1d}} + p_{u_{1u}} C_{u_{1d}} + p_{u_{2u}} D_{u_{1d}} + \sigma_{u_{1d}}^2} \right\} \right) \quad (40)$$

1- The average of the first term  $A_{u_{1d}}$  can be calculated, after removing the zero expectation terms, as

$$\begin{aligned} & \mathcal{E} \left\{ \left| \sqrt{l_{b,u_{1d}}^{-m}} h_{b,u_{1d}} + \sqrt{l_{b,r}^{-m} l_{r,u_{1d}}^{-m}} \mathbf{g}_{r,u_{1d}} \Theta \mathbf{g}_{b,r} \right|^2 \right\} = \\ & \mathcal{E} \left\{ l_{b,u_{1d}}^{-m} |h_{b,u_{1d}}|^2 \right\} + l_{b,r}^{-m} \mathcal{E} \left\{ l_{r,u_{1d}}^{-m} \right\} \mathcal{E} \left\{ |\mathbf{g}_{r,u_{1d}} \Theta \mathbf{g}_{b,r}|^2 \right\} \end{aligned} \quad (41)$$

The first expectation,  $\mathcal{E} \left\{ l_{b,u_{1d}}^{-m} |h_{b,u_{1d}}|^2 \right\} = \mathcal{E} \left\{ l_{b,u_{1d}}^{-m} \right\}$ . The probability density function (PDF) of the strong user at distance  $r$  relative to the BS is  $f_d(r) = \frac{2r}{R^2}$  [38]. Thus we can get,

$$\mathcal{E} \left\{ l_{b,u_{1d}}^{-m} \right\} = \int_0^R (1 + r_{b,u_{1d}})^{-m} \frac{2(r_{b,u_{1d}})}{(R)^2} dr_{b,u_{1d}} =$$

$$\frac{2(1+R)^{-m}(-1+R^2+mR(1+R)+(1+R)^m)}{(m-2)(m-1)R^2} \quad (42)$$

The second expectation, considering the distribution of the distance between a fixed point outside a circle and a random point inside the circle in [39], we can write

$$\begin{aligned} \mathcal{E} \{l_{r,u_{1d}}^{-m}\} &= \int_{r_1}^{r_1+2R} r_{r,u_{1d}}^{-m} \frac{2r_{r,u_{1d}}}{\pi R^2} \cos^{-1} \left( \frac{1}{r_{r,u_{1d}}} \right. \\ &\quad \left. \left( r_1 + \frac{(r_{r,u_{1d}}^2 - r_1^2)}{2(R+r_1)} \right) \right) dr_{r,u_{1d}} \end{aligned} \quad (43)$$

where  $r_1 \leq r_{r,u_{1d}} \leq r_1 + 2R$ ,  $r_1 = d_{b,r} - R$ . Using Gaussian Quadrature rules we can get

$$\begin{aligned} \mathcal{E} \{l_{r,u_{1d}}^{-m}\} &= \sum_{j=1}^C H_j (1 + (Rr_j + R))^{-m} \frac{2(Rr_j + R)}{\pi R^2} \\ &\quad \times \cos^{-1} \left( \frac{1}{(Rr_j + R)} \left( r_1 + \frac{((Rr_j + R)^2 - r_1^2)}{2(R+r_1)} \right) \right) \end{aligned} \quad (44)$$

where  $r_j$  and  $H_j$  are the  $j^{\text{th}}$  zero and the weighting factor of the Laguerre polynomials, respectively [40]. The last expectation can be written after removing the zero expectation terms as

$$\begin{aligned} \mathcal{E} \left\{ \left| \mathbf{g}_{r,u_{1d}} \Theta \mathbf{g}_{b,r} \right|^2 \right\} &= \frac{\kappa_{r,u_{1d}}}{\kappa_{r,u_{1d}} + 1} \frac{\kappa_{b,r}}{\kappa_{b,r} + 1} \mathcal{E} \left| \bar{\mathbf{g}}_{r,u_{1d}} \Theta \bar{\mathbf{g}}_{b,r} \right|^2 + \frac{\kappa_{r,u_{1d}}}{\kappa_{r,u_{1d}} + 1} \frac{1}{\kappa_{b,r} + 1} \mathcal{E} \left| \bar{\mathbf{g}}_{r,u_{1d}} \Theta \tilde{\mathbf{g}}_{b,r} \right|^2 \\ &\quad + \frac{\kappa_{b,r}}{\kappa_{b,r} + 1} \frac{1}{\kappa_{r,u_{1d}} + 1} \mathcal{E} \left| \tilde{\mathbf{g}}_{r,u_{1d}} \Theta \bar{\mathbf{g}}_{b,r} \right|^2 + \frac{1}{\kappa_{r,u_{1d}} + 1} \frac{1}{\kappa_{b,r} + 1} \mathcal{E} \left| \tilde{\mathbf{g}}_{r,u_{1d}} \Theta \tilde{\mathbf{g}}_{b,r} \right|^2 \end{aligned} \quad (45)$$

Now, the first term in (45) is

$$\mathcal{E} \left| \bar{\mathbf{g}}_{r,u_{1d}} \Theta \bar{\mathbf{g}}_{b,r} \right|^2 =$$

$$\left| \sum_{n=1}^N a_{N,n} (\psi_{b,r}^a, \psi_{b,r}^e) \rho_n^k e^{j\phi_n^k} a_{N,n} (\psi_{r,u_{1d}}^a, \psi_{r,u_{1d}}^e) \right|^2 = \xi_1 \quad (46)$$

Similarly, the second term,

$$\begin{aligned} \mathcal{E} \left| \bar{\mathbf{g}}_{r,u_{1d}} \Theta \tilde{\mathbf{g}}_{b,r} \right|^2 &= \sum_{n=1}^N |\rho_n^k|^2 + \\ \mathcal{E} \left\{ \sum_{n_1=1}^N \sum_{n_2 \neq n_1}^N \left( a_{Nn_1} (\psi_{r,u_{1d}}^a, \psi_{r,u_{1d}}^e) \rho_{n_1}^k e^{j\phi_{n_1}^k} [\tilde{\mathbf{g}}_{b,r}]_{n_1} \right) \right. \\ \left. \left( a_{Nn_2} (\psi_{r,u_{1d}}^a, \psi_{r,u_{1d}}^e) \rho_{n_2}^k e^{j\phi_{n_2}^k} [\tilde{\mathbf{g}}_{b,r}]_{n_2} \right)^H \right\} &= \sum_{n=1}^N |\rho_n^k|^2 \end{aligned} \quad (47)$$

The third term,

$$\begin{aligned} \mathcal{E} \left| \tilde{\mathbf{g}}_{r,u_{1d}} \Theta \bar{\mathbf{g}}_{b,r} \right|^2 &= \sum_{n=1}^N |\rho_n^k|^2 + \\ \mathcal{E} \left\{ \sum_{n_1=1}^N \sum_{n_2 \neq n_1}^N \left( [\tilde{\mathbf{g}}_{r,u_{1d}}]_{n_1} \rho_{n_1}^k e^{j\phi_{n_1}^k} a_{Nn_1} (\psi_{b,r}^a, \psi_{b,r}^e) \right) \right. \\ \left. \left( [\tilde{\mathbf{g}}_{r,u_{1d}}]_{n_2} \rho_{n_2}^k e^{j\phi_{n_2}^k} a_{Nn_2} (\psi_{b,r}^a, \psi_{b,r}^e) \right)^H \right\} &= \sum_{n=1}^N |\rho_n^k|^2 \end{aligned} \quad (48)$$

The last term,

$$\begin{aligned} \mathcal{E} \left| \tilde{\mathbf{g}}_{r,u_{1d}} \Theta \tilde{\mathbf{g}}_{b,r} \right|^2 &= \\ \mathcal{E} \left| \sum_{n=1}^N [\tilde{\mathbf{g}}_{r,u_{1d}}]_n \rho_n^k e^{j\phi_n^k} [\tilde{\mathbf{g}}_{b,r}]_n \right|^2 &= \sum_{n=1}^N |\rho_n^k|^2 \end{aligned} \quad (49)$$

Now, we are ready to write the average as

$$\begin{aligned}
\mathcal{E} \{ |\mathbf{g}_{r,u_{1d}} \Theta \mathbf{g}_{b,r}|^2 \} &= \frac{\kappa_{r,u_{1d}}}{\kappa_{r,u_{1d}} + 1} \frac{\kappa_{b,r}}{\kappa_{b,r} + 1} \xi_1 \\
&+ \frac{\kappa_{r,u_{1d}}}{\kappa_{r,u_{1d}} + 1} \frac{\sum_{n=1}^N |\rho_n^k|^2}{\kappa_{b,r} + 1} + \frac{\kappa_{b,r}}{\kappa_{b,r} + 1} \frac{\sum_{n=1}^N |\rho_n^k|^2}{\kappa_{r,u_{1d}} + 1} \\
&+ \frac{1}{\kappa_{r,u_{1d}} + 1} \frac{1}{\kappa_{b,r} + 1} \sum_{n=1}^N |\rho_n^k|^2
\end{aligned} \tag{50}$$

2- The average of the term  $C_{u_{1d}}$  can be calculated by

$$\begin{aligned}
&\mathcal{E} \left\{ \left| \sqrt{l_{u_{1d},u_{1u}}^{-m}} h_{u_{1d},u_{1u}} + \sqrt{l_{r,u_{1u}}^{-m} l_{r,u_{1d}}^{-m}} \mathbf{g}_{r,u_{1d}} \Theta \mathbf{g}_{r,u_{1u}} \right|^2 \right\} \\
&= \mathcal{E} \{ l_{u_{1d},u_{1u}}^{-m} |h_{u_{1d},u_{1u}}|^2 \} + \mathcal{E} \{ l_{r,u_{1u}}^{-m} l_{r,u_{1d}}^{-m} |\mathbf{g}_{r,u_{1d}} \Theta \mathbf{g}_{r,u_{1u}}|^2 \}
\end{aligned} \tag{51}$$

The first expectation  $\mathcal{E} \{ l_{u_{1d},u_{1u}}^{-m} |h_{u_{1d},u_{1u}}|^2 \} = \mathcal{E} \{ l_{u_{1d},u_{1u}}^{-m} \}$ . Considering the distribution of the distance between two random points inside a circle in [39], we can write

$$\begin{aligned}
\mathcal{E} \{ l_{u_{1d},u_{1u}}^{-m} \} &= \int_{r_0}^{2R} (1 + r_{u_{1d},u_{1u}})^{-m} \frac{4r_{u_{1d},u_{1u}}}{\pi R^2} \times \\
&\left( \cos^{-1} \left( \frac{r_{u_{1d},u_{1u}}}{2R} \right) - \frac{r_{u_{1d},u_{1u}}}{2R} \left( \sqrt{1 - \frac{r_{u_{1d},u_{1u}}^2}{4R^2}} \right) \right) dr_{u_{1d},u_{1u}}
\end{aligned} \tag{52}$$

which can be found as

$$\begin{aligned}
\mathcal{E} \{ l_{u_{1d},u_{1u}}^{-m} \} &= \frac{2}{(2 - 3m + m^2) R^2} - \\
&\frac{2F \left( \left\{ \frac{1}{2}, -1 + \frac{m}{2}, -\frac{1}{2} + \frac{m}{2} \right\}, \left\{ \frac{-1}{2}, 1 \right\}, 4R^2 \right)}{(2 - 3m + m^2) R^2}
\end{aligned}$$

$$\begin{aligned}
& -F\left(\left\{\frac{3}{2}, \frac{1}{2} + \frac{m}{2}, \frac{m}{2}\right\}, \left\{\frac{1}{2}, 3\right\}, 4R^2\right) \\
& + \frac{64mRF\left(\left\{2, \frac{1}{2} + \frac{m}{2}, 1 + \frac{m}{2}\right\}, \left\{\frac{3}{2}, \frac{7}{2}\right\}, 4R^2\right)}{15\pi} \\
& - \frac{64mRF\left(\left\{2, \frac{1}{2} + \frac{m}{2}, 1 + \frac{m}{2}\right\}, \left\{\frac{5}{2}, \frac{5}{2}\right\}, 4R^2\right)}{9\pi}
\end{aligned} \tag{53}$$

where  $F(\cdot)$  is Hypergeometric function. The second expectation,  $\mathcal{E}\{l_{r,u_{1d}}^{-m}\}$  is derived in (43) and (44). Similar to the derivation in (43) and (45) we can get

$$\begin{aligned}
\mathcal{E}\{l_{r,u_{1u}}^{-m}\} &= \sum_{j=1}^C \mathbf{H}_j (1 + (Rr_j + R))^{-m} \frac{2(Rr_j + R)}{\pi R^2} \\
&\times \cos^{-1}\left(\frac{1}{(Rr_j + R)} \left(r_1 + \frac{((Rr_j + R)^2 - r_1^2)}{2(R + r_1)}\right)\right)
\end{aligned} \tag{54}$$

and

$$\begin{aligned}
\mathcal{E}\left\{|\mathbf{g}_{r,u_{1d}} \Theta \mathbf{g}_{r,u_{1u}}|^2\right\} &= \frac{\kappa_{r,u_{1d}}}{\kappa_{r,u_{1d}} + 1} \frac{\kappa_{r,u_{1u}}}{\kappa_{r,u_{1u}} + 1} \xi_2 \\
&+ \frac{\kappa_{r,u_{1d}}}{\kappa_{r,u_{1d}} + 1} \frac{\sum_{n=1}^N |\rho_n^k|^2}{\kappa_{r,u_{1u}} + 1} + \frac{\kappa_{r,u_{1u}}}{\kappa_{r,u_{1u}} + 1} \frac{\sum_{n=1}^N |\rho_n^k|^2}{\kappa_{r,u_{1d}} + 1} \\
&+ \frac{1}{\kappa_{r,u_{1d}} + 1} \frac{\sum_{n=1}^N |\rho_n^k|^2}{\kappa_{r,u_{1u}} + 1}
\end{aligned} \tag{55}$$

where  $\xi_2 = |\bar{\mathbf{g}}_{r,u_{1d}} \Theta \bar{\mathbf{g}}_{r,u_{1u}}|^2$ .

3- The average of the term  $D_{u_{1d}}$  can be calculated by

$$\mathcal{E}\{l_{r,u_{2u}}^{-m} l_{r,u_{1d}}^{-m} |\mathbf{g}_{r,u_{1d}} \Theta \mathbf{g}_{r,u_{2u}}|^2\} =$$



$$\mathcal{E} \{l_{r,u_{2u}}^{-m}\} \mathcal{E} \{l_{r,u_{1d}}^{-m}\} \mathcal{E} \{|\mathbf{g}_{r,u_{1d}} \Theta \mathbf{g}_{r,u_{2u}}|^2\} \quad (56)$$

The PDF of the weak user at radius  $r_r$  relative to the RIS is  $f_d(r_r) = \frac{2r_r}{R_r^2}$ , [38]. Thus, we can get

$$\begin{aligned} \mathcal{E} \{l_{r,u_{2u}}^{-m}\} &= \frac{2(1+R_r)^{-m}}{(m-2)(m-1)R_r^2} \\ &\times (-1 + R_r^2 + mR_r(1+R_r) + (1+R_r)^m) \end{aligned} \quad (57)$$

where  $\mathcal{E} \{l_{r,u_{1d}}^{-m}\}$  is derived in (43) and (44). Similar to the derivation in (45) we can obtain

$$\begin{aligned} \mathcal{E} \left\{ |\mathbf{g}_{r,u_{1d}} \Theta \mathbf{g}_{u_{2u},r}|^2 \right\} &= \frac{\kappa_{r,u_{1d}}}{\kappa_{r,u_{1d}} + 1} \frac{\kappa_{r,u_{2u}}}{\kappa_{r,u_{2u}} + 1} \xi_3 + \\ &\frac{\kappa_{r,u_{1d}}}{\kappa_{r,u_{1d}} + 1} \frac{\sum_{n=1}^N |\rho_n^k|^2}{\kappa_{r,u_{2u}} + 1} + \frac{\kappa_{r,u_{2u}}}{\kappa_{r,u_{2u}} + 1} \frac{\sum_{n=1}^N |\rho_n^k|^2}{\kappa_{r,u_{1d}} + 1} \\ &+ \frac{1}{\kappa_{r,u_{1d}} + 1} \frac{\sum_{n=1}^N |\rho_n^k|^2}{\kappa_{r,u_{2u}} + 1} \end{aligned} \quad (58)$$

where  $\xi_3 = |\bar{\mathbf{g}}_{r,u_{1d}} \Theta \bar{\mathbf{g}}_{r,u_{2u}}|^2$ .

## APPENDIX B

By using Jensen inequality, the ergodic rate can be expressed as

$$\mathcal{E} [R_{u_{2d}}] \approx \log_2 \left( 1 + \mathcal{E} \left[ \frac{P_{b_2} A_{u_{2d}}}{P_{b_1} A_{u_{2d}} + p_{u_{1u}} C_{u_{2d}} + p_{u_{2u}} D_{u_{2d}} + \sigma_{u_{2d}}^2} \right] \right) \quad (59)$$

1- The average of the first term  $A_{u_{2d}}$  can be calculated by

$$\mathcal{E} \left\{ l_{b,r}^{-m} l_{r,u_{2d}}^{-m} |\mathbf{g}_{r,u_{2d}} \Theta_r \mathbf{g}_{b,r}|^2 \right\} =$$

$$l_{b,r}^{-m} \mathcal{E} \{ l_{r,u2d}^{-m} \} \mathcal{E} \left\{ \left| \mathbf{g}_{r,u2d} \Theta_r \mathbf{g}_{b,r} \right|^2 \right\} \quad (60)$$

The PDF of the weak user at radius  $r_r$  relative to the RIS is  $f_d(r_r) = \frac{2r_r}{R_r^2}$ , [38]. Thus,

$$\begin{aligned} \mathcal{E} \{ l_{r,u2d}^{-m} \} &= \int_0^{R_r} (1 + r_{r,u2d})^{-m} \frac{2(r_{r,u2d})}{R_r^2} dr_{r,u2d} = \\ &= \frac{2(1 + R_r)^{-m}}{(m-2)(m-1)R_r^2} \times \\ &= (R_r^2 + mR_r(1 + R_r) + (1 + R_r)^m - 1) \end{aligned} \quad (61)$$

Now the average of the other term can be derived as in Appendix A as,

$$\begin{aligned} \mathcal{E} \left\{ \left| \mathbf{g}_{r,u2d} \Theta \mathbf{g}_{b,r} \right|^2 \right\} &= \frac{\kappa_{r,u2d}}{\kappa_{r,u2d} + 1} \frac{\kappa_{b,r}}{\kappa_{b,r} + 1} \xi_4 \\ &+ \frac{\kappa_{r,u2d}}{\kappa_{r,u2d} + 1} \frac{\sum_{n=1}^N |\rho_n^k|^2}{\kappa_{b,r} + 1} + \frac{\kappa_{b,r}}{\kappa_{b,r} + 1} \frac{\sum_{n=1}^N |\rho_n^k|^2}{\kappa_{r,u2d} + 1} \\ &+ \frac{1}{\kappa_{r,u2d} + 1} \frac{1}{\kappa_{b,r} + 1} \sum_{n=1}^N |\rho_n^k|^2 \end{aligned} \quad (62)$$

where  $\xi_4 = \left| \bar{\mathbf{g}}_{r,u2d} \Theta \bar{\mathbf{g}}_{b,r} \right|^2$ .

2- The average of the second term,  $C_{u2d}$ , can be calculated by

$$\begin{aligned} \mathcal{E} \left\{ l_{r,u2d}^{-m} l_{r,u1u}^{-m} \left| \mathbf{g}_{r,u2d} \Theta_k \mathbf{g}_{r,u1u} \right|^2 \right\} &= \\ \mathcal{E} \{ l_{r,u2d}^{-m} \} \mathcal{E} \{ l_{r,u1u}^{-m} \} \mathcal{E} \left\{ \left| \mathbf{g}_{r,u2d} \Theta_k \mathbf{g}_{r,u1u} \right|^2 \right\} \end{aligned} \quad (63)$$

The term  $\mathcal{E} \{ l_{r,u2d}^{-m} \}$  is derived in (61). Considering the distribution of the distance between a

fixed point outside and a random point inside a circle in [39], we can obtain the average of the second term as

$$\mathcal{E} \{l_{r,u1u}^{-m}\} = \int_{r_1}^{r_1+2R} r_{r,u1u}^{-m} \frac{2r_{r,u1u}}{\pi R^2} \times \cos^{-1} \left( \frac{1}{r_{r,u1u}} \left( r_1 + \frac{(r_{r,u1u}^2 - r_1^2)}{2(R+r_1)} \right) \right) dr_{r,u1u} \quad (64)$$

where  $r_1 \leq r_{r,u1u} \leq r_1 + 2R$ ,  $r_1 = d_{b,r} - R$  is the distance from RIS to the boundary. The last expression can be rewritten as,

$$\mathcal{E} \{l_{r,u1u}^{-m}\} = \sum_{j=1}^C H_j (1 + (Rr_j + R))^{-m} \frac{2(Rr_j + R)}{\pi R^2} \cos^{-1} \left( \frac{1}{(Rr_j + R)} \left( r_1 + \frac{((Rr_j + R)^2 - r_1^2)}{2(R+r_1)} \right) \right) \quad (65)$$

The average of the last term is

$$\begin{aligned} \mathcal{E} \left\{ |\mathbf{g}_{r,u2d} \Theta_k \mathbf{g}_{r,u1u}|^2 \right\} &= \frac{\kappa_{r,u2d}}{\kappa_{r,u2d} + 1} \frac{\kappa_{r,u1u}}{\kappa_{r,u1u} + 1} \xi_5 + \\ &+ \frac{\kappa_{r,u2d}}{\kappa_{r,u2d} + 1} \frac{\sum_{n=1}^N |\rho_n^k|^2}{\kappa_{r,u1u} + 1} + \frac{\kappa_{u1u,r}}{\kappa_{u1u,r} + 1} \frac{\sum_{n=1}^N |\rho_n^k|^2}{\kappa_{r,u2d} + 1} \\ &+ \frac{1}{\kappa_{r,u2d} + 1} \frac{1}{\kappa_{r,u1u} + 1} \sum_{n=1}^N |\rho_n^k|^2 \end{aligned} \quad (66)$$

where  $\xi_5 = |\bar{\mathbf{g}}_{r,u2d} \Theta \bar{\mathbf{g}}_{r,u1u}|^2$ .

3- The average of the third term,  $D_{u2d}$ , can be derived as

$$\mathcal{E} \left\{ l_{r,u2d}^{-m} l_{r,u2u}^{-m} |\mathbf{g}_{r,u2d} \Theta \mathbf{g}_{r,u2u}|^2 \right\} =$$

$$\mathcal{E} \{l_{r,u2d}^{-m}\} \mathcal{E} \{l_{r,u2u}^{-m}\} \mathcal{E} \left\{ \left| \mathbf{g}_{r,u2d} \Theta \mathbf{g}_{r,u2u} \right|^2 \right\} \quad (67)$$

The term  $\mathcal{E} \{l_{r,u2d}^{-m}\}$  is derived in (61). Following the derivation in (61) we can get

$$\begin{aligned} \mathcal{E} \{l_{r,u2u}^{-m}\} &= \frac{2(1+R_r)^{-m}}{(m-2)(m-1)R_r^2} \times \\ &(-1+R_r^2+mR_r(1+R_r)+(1+R_r)^m) \end{aligned} \quad (68)$$

and

$$\begin{aligned} \mathcal{E} \left\{ \left| \mathbf{g}_{r,u2d} \Theta \mathbf{g}_{r,u2u} \right|^2 \right\} &= \frac{\kappa_{r,u2d}}{\kappa_{r,u2d}+1} \frac{\kappa_{r,u2u}}{\kappa_{r,u2u}+1} \xi_6 + \\ &\frac{\kappa_{r,u2d}}{\kappa_{r,u2d}+1} \frac{\sum_{n=1}^N |\rho_n^k|^2}{\kappa_{r,u2u}+1} + \frac{\kappa_{r,u1u}}{\kappa_{r,u1u}+1} \frac{\sum_{n=1}^N |\rho_n^k|^2}{\kappa_{r,u2u}+1} \\ &+ \frac{1}{\kappa_{r,u2d}+1} \frac{1}{\kappa_{r,u2u}+1} \sum_{n=1}^N |\rho_n^k|^2 \end{aligned} \quad (69)$$

where  $\xi_6 = \left| \bar{\mathbf{g}}_{r,u2d} \Theta \bar{\mathbf{g}}_{r,u2u} \right|^2$ .

## APPENDIX C

By using Jensen inequality, the ergodic rate can be expressed as

$$\mathcal{E} [R_{u1u}] \approx \log_2 \left( 1 + \mathcal{E} \left\{ \frac{p_{u1u} A_{u1u}}{p_{u2u} B_{u1u} + P_b C_{u1u} + |\tilde{s}|^2 + \sigma_b^2} \right\} \right) \quad (70)$$

1- The average of the first term,  $A_{u1u}$ , can be derived as

$$\mathcal{E} \left\{ \left| \sqrt{l_{b,u1u}^{-m}} h_{b,u1u} + \sqrt{l_{b,r}^{-m} l_{r,u1u}^{-m}} \mathbf{g}_{b,r} \Theta \mathbf{g}_{r,u1u} \right|^2 \right\} =$$

$$p_{u_{1u}} \mathcal{E} \left| \sqrt{l_{b,u_{1u}}^{-m}} h_{b,u_{1u}} \right|^2 + \mathcal{E} \left| \sqrt{l_{b,r}^{-m} l_{r,u_{1u}}^{-m}} \mathbf{g}_{b,r} \Theta \mathbf{g}_{r,u_{1u}} \right|^2 \quad (71)$$

The first expectation,  $\mathcal{E} \{ l_{b,u_{1u}}^{-m} |h_{b,u_{1u}}|^2 \} = \mathcal{E} \{ l_{b,u_{1u}}^{-m} \}$ . The PDF of the weak user at radius  $r$  relative to the RIS is  $f_d(r) = \frac{2r}{R^2}$ , [38]. Thus,

$$\begin{aligned} \mathcal{E} \{ l_{b,u_{1u}}^{-m} \} &= \int_0^R (1 + r_{b,u_{1u}})^{-m} \frac{2(r_{b,u_{1u}})}{(R)^2} dr_{b,u_{1u}} \\ &= \frac{2(1+R)^{-m}}{(m-2)(m-1)R^2} \times \\ &\quad (R^2 + mR(1+R) + (1+R)^m - 1) \end{aligned} \quad (72)$$

The second term,

$$\begin{aligned} \mathcal{E} \left\{ \left| \sqrt{l_{b,r}^{-m} l_{r,u_{1u}}^{-m}} \mathbf{g}_{b,r} \Theta \mathbf{g}_{r,u_{1u}} \right|^2 \right\} &= \\ l_{b,r}^{-m} \mathcal{E} \left\{ l_{r,u_{1u}}^{-m} \left| \mathbf{g}_{b,r} \Theta \mathbf{g}_{r,u_{1u}} \right|^2 \right\} \end{aligned} \quad (73)$$

in which  $\mathcal{E} \{ l_{r,u_{1u}}^{-m} \}$  is derived in (64) and (65). The average of the last term can be found as,

$$\begin{aligned} \mathcal{E} \left\{ \left| \mathbf{g}_{b,r} \Theta \mathbf{g}_{r,u_{1u}} \right|^2 \right\} &= \frac{\kappa_{r,u_{1u}}}{\kappa_{r,u_{1u}} + 1} \frac{\kappa_{b,r}}{\kappa_{b,r} + 1} \xi_7 + \\ &\quad \frac{\kappa_{r,u_{1u}}}{\kappa_{r,u_{1u}} + 1} \frac{\sum_{n=1}^N |\rho_n^k|^2}{\kappa_{b,r} + 1} + \frac{\kappa_{b,r}}{\kappa_{b,r} + 1} \frac{\sum_{n=1}^N |\rho_n^k|^2}{\kappa_{r,u_{1u}} + 1} \\ &\quad + \frac{1}{\kappa_{r,u_{1u}} + 1} \frac{1}{\kappa_{b,r} + 1} \sum_{n=1}^N |\rho_n^k|^2 \end{aligned} \quad (74)$$

where  $\xi_7 = \left| \bar{\mathbf{g}}_{b,r} \Theta \bar{\mathbf{g}}_{r,u_{1u}} \right|^2$ .

2- The average of the second term,  $B_{u_{1u}}$ , can be obtained as

$$\begin{aligned} \mathcal{E} \left\{ l_{b,r}^{-m} l_{r,u_{2u}}^{-m} \left| \mathbf{g}_{b,r} \Theta \mathbf{g}_{r,u_{2u}} \right|^2 \right\} = \\ l_{b,r}^{-m} \mathcal{E} \left\{ l_{r,u_{2u}}^{-m} \right\} \mathcal{E} \left\{ \left| \mathbf{g}_{b,r} \Theta \mathbf{g}_{r,u_{2u}} \right|^2 \right\} \end{aligned} \quad (75)$$

in which  $\mathcal{E} \left\{ l_{r,u_{2u}}^{-m} \right\}$  is derived in (68). The average of the other term can be calculated as

$$\begin{aligned} \mathcal{E} \left\{ \left| \mathbf{g}_{b,r} \Theta \mathbf{g}_{r,u_{2u}} \right|^2 \right\} = \frac{\kappa_{r,u_{2u}}}{\kappa_{r,u_{2u}} + 1} \frac{\kappa_{b,r}}{\kappa_{b,r} + 1} \xi_8 + \\ \frac{\kappa_{r,u_{2u}}}{\kappa_{r,u_{2u}} + 1} \frac{\sum_{n=1}^N |\rho_n^k|^2}{\kappa_{b,r} + 1} + \frac{\kappa_{b,r}}{\kappa_{b,r} + 1} \frac{\sum_{n=1}^N |\rho_n^k|^2}{\kappa_{r,u_{2u}} + 1} \\ + \frac{1}{\kappa_{r,u_{2u}} + 1} \frac{1}{\kappa_{b,r} + 1} \sum_{n=1}^N |\rho_n^k|^2 \end{aligned} \quad (76)$$

where  $\xi_8 = \left| \bar{\mathbf{g}}_{b,r} \Theta \bar{\mathbf{g}}_{r,u_{2u}} \right|^2$ .

3- The average of the third term,  $C_{u_{1u}}$  can be derived as

$$\begin{aligned} \mathcal{E} \left\{ l_{b,r}^{-m} l_{b,r}^{-m} \left| \mathbf{g}_{b,r} \Theta_k \mathbf{g}_{b,r}^H \right|^2 \right\} = \\ l_{b,r}^{-m} l_{b,r}^{-m} \mathcal{E} \left\{ \left| \mathbf{g}_{b,r} \Theta_k \mathbf{g}_{b,r}^H \right|^2 \right\} \end{aligned} \quad (77)$$

The average can be written as

$$\mathcal{E} \left\{ \left| \mathbf{g}_{b,r} \Theta_k \mathbf{g}_{b,r}^H \right|^2 \right\} = \mathcal{E} \left\{ \left| \left( \sqrt{\frac{\kappa_{b,r}}{\kappa_{b,r} + 1}} \sqrt{\frac{\kappa_{b,r}}{\kappa_{b,r} + 1}} \bar{\mathbf{g}}_{b,r} \Theta \bar{\mathbf{g}}_{b,r}^H + \sqrt{\frac{\kappa_{b,r}}{\kappa_{b,r} + 1}} \sqrt{\frac{1}{\kappa_{b,r} + 1}} \bar{\mathbf{g}}_{b,r} \Theta \tilde{\mathbf{g}}_{b,r}^H \right. \right. \right.$$

$$+ \left. \sqrt{\frac{\kappa_{b,r}}{\kappa_{b,r}+1}} \sqrt{\frac{1}{\kappa_{b,r}+1}} \tilde{\mathbf{g}}_{b,r} \Theta \bar{\mathbf{g}}_{b,r}^H + \sqrt{\frac{1}{\kappa_{b,r}+1}} \sqrt{\frac{1}{\kappa_{b,r}+1}} \tilde{\mathbf{g}}_{b,r} \Theta \tilde{\mathbf{g}}_{b,r}^H \right\}^2 \quad (78)$$

$$\begin{aligned} \mathcal{E} \left\{ |\mathbf{g}_{b,r} \Theta \mathbf{g}_{b,r}^H|^2 \right\} &= \left( \frac{\kappa_{b,r}}{\kappa_{b,r}+1} \right)^2 \mathcal{E} |\bar{\mathbf{g}}_{b,r} \Theta \bar{\mathbf{g}}_{b,r}^H|^2 + \frac{\kappa_{b,r}}{\kappa_{b,r}+1} \frac{1}{\kappa_{b,r}+1} \mathcal{E} |\bar{\mathbf{g}}_{b,r} \Theta \tilde{\mathbf{g}}_{b,r}^H|^2 \\ &+ \frac{\kappa_{b,r}}{\kappa_{b,r}+1} \frac{1}{\kappa_{b,r}+1} \mathcal{E} |\tilde{\mathbf{g}}_{b,r} \Theta \bar{\mathbf{g}}_{b,r}^H|^2 + \left( \frac{1}{\kappa_{b,r}+1} \right)^2 \mathcal{E} |\tilde{\mathbf{g}}_{b,r} \Theta \tilde{\mathbf{g}}_{b,r}^H|^2 + 2 \frac{\kappa_{b,r}}{\kappa_{b,r}+1} \frac{1}{\kappa_{b,r}+1} \mathcal{E} (\bar{\mathbf{g}}_{b,r} \Theta \bar{\mathbf{g}}_{b,r}^H \tilde{\mathbf{g}}_{b,r}^H \Theta \tilde{\mathbf{g}}_{b,r}^H) \end{aligned} \quad (79)$$

The first term in (79) can be found as  $\mathcal{E} |\bar{\mathbf{g}}_{b,r} \Theta \bar{\mathbf{g}}_{b,r}^H|^2 = |\bar{\mathbf{g}}_{b,r} \Theta \bar{\mathbf{g}}_{b,r}^H|^2 = \xi_g$ . Similarly, the second term,

$$\bar{\mathbf{g}}_{b,r} \Theta \tilde{\mathbf{g}}_{b,r}^H = \mathbf{a}_N (\psi_{b,r}^a, \psi_{b,r}^e) \Theta \tilde{\mathbf{g}}_{b,r}^H$$

$$= \sum_{n=1}^N a_{Nn} (\psi_{b,r}^a, \psi_{b,r}^e) \rho_n^k e^{j\phi_n^k} [\tilde{\mathbf{g}}_{b,r}]_n \quad (80)$$

$$\mathcal{E} |\bar{\mathbf{g}}_{b,r} \Theta \tilde{\mathbf{g}}_{b,r}^H|^2 = \sum_{n=1}^N |\rho_n^k|^2 +$$

$$\mathcal{E} \left\{ \sum_{n_1=1}^N \sum_{n_2 \neq n_1}^N \left( a_{Nn_1} (\psi_{b,r}^a, \psi_{b,r}^e) \rho_{n_1}^k e^{j\phi_{n_1}^k} [\tilde{\mathbf{g}}_{b,r}]_{n_1} \right) \right.$$

$$\left. \times \left( a_{Nn_2} (\psi_{b,r}^a, \psi_{b,r}^e) \rho_{n_2}^k e^{j\phi_{n_2}^k} [\tilde{\mathbf{g}}_{b,r}]_{n_2} \right)^H \right\} = \sum_{n=1}^N |\rho_n^k|^2 \quad (81)$$

The other terms,  $\tilde{\mathbf{g}}_{b,r} \Theta \bar{\mathbf{g}}_{b,r}^H = \sum_{n=1}^N [\tilde{\mathbf{g}}_{b,r}]_n \rho_n^k e^{j\phi_n^k} a_{N,n} (\psi_{b,r}^a, \psi_{b,r}^e)$ , so we can write,

$$\mathcal{E} |\tilde{\mathbf{g}}_{b,r} \Theta \bar{\mathbf{g}}_{b,r}^H|^2 = \sum_{n=1}^N |\rho_n^k|^2 +$$

$$\begin{aligned} & \mathcal{E} \left\{ \sum_{n_1=1}^N \sum_{n_2 \neq n_1}^N \left( [\tilde{\mathbf{g}}_{b,r}]_{n_1} \rho_{n_1}^k e^{j\phi_{n_1}^k} a_{Nn_1} (\psi_{b,r}^a, \psi_{b,r}^e) \right) \right. \\ & \left. \times \left( [\tilde{\mathbf{g}}_{b,r}]_{n_2} \rho_{n_2}^k e^{j\phi_{n_2}^k} a_{Nn_2} (\psi_{b,r}^a, \psi_{b,r}^e) \right)^H \right\} = \sum_{n=1}^N |\rho_n^k|^2 \end{aligned} \quad (82)$$

and  $\tilde{\mathbf{g}}_{b,r} \Theta \tilde{\mathbf{g}}_{b,r}^H = \sum_{n=1}^N [\tilde{\mathbf{g}}_{b,r}]_n \rho_n^k e^{j\phi_n^k} [\tilde{\mathbf{g}}_{b,r}^H]_n$ , so we can get

$$\mathcal{E} |\tilde{\mathbf{g}}_{b,r} \Theta \tilde{\mathbf{g}}_{b,r}^H|^2 = \mathcal{E} \left| \sum_{n=1}^N [\tilde{\mathbf{g}}_{b,r}]_n \rho_n^k e^{j\phi_n^k} [\tilde{\mathbf{g}}_{b,r}^H]_n \right|^2 \quad (83)$$

$$\mathcal{E} |\tilde{\mathbf{g}}_{b,r} \Theta \tilde{\mathbf{g}}_{b,r}^H|^2 = 2 \sum_{n=1}^N |\rho_n^k|^2 +$$

$$\mathcal{E} \left\{ \sum_{n_1=1}^N \sum_{n_2 \neq n_1}^N \left( [\tilde{\mathbf{g}}_{b,r}]_{n_1} \rho_{n_1}^k e^{j\phi_{n_1}^k} [\tilde{\mathbf{g}}_{b,r}^H]_{n_1} \right) \right. \\ \left. \left( [\tilde{\mathbf{g}}_{b,r}]_{n_2} \rho_{n_2}^k e^{j\phi_{n_2}^k} [\tilde{\mathbf{g}}_{b,r}^H]_{n_2} \right)^H \right\}$$

$$= 2 \sum_{n=1}^N |\rho_n^k|^2 + \sum_{n_1=1}^N \sum_{n_2 \neq n_1}^N \left( \rho_{n_1}^k e^{j\phi_{n_1}^k} \right) \left( \rho_{n_2}^k e^{j\phi_{n_2}^k} \right)^H \quad (84)$$

The last term

$$\bar{\mathbf{g}}_{b,r} \Theta \bar{\mathbf{g}}_{b,r}^H \tilde{\mathbf{g}}_{b,r} \Theta \tilde{\mathbf{g}}_{b,r}^H =$$

$$\sum_{n=1}^N a_{Nn} (\psi_{b,r}^a, \psi_{b,r}^e)^H \rho_n^k e^{j\phi_n^k} a_{Nn} (\psi_{b,r}^a, \psi_{b,r}^e) \sum_{n=1}^N \left( \rho_n^k e^{j\phi_n^k} \right)^H \quad (85)$$

Now we can write the average as,

$$\mathcal{E} \left\{ |\mathbf{g}_{b,r} \Theta \mathbf{g}_{b,r}^H|^2 \right\} = \left( \frac{\kappa_{b,r}}{\kappa_{b,r} + 1} \right)^2 \xi_9$$



$$\begin{aligned}
& +2 \frac{\kappa_{b,r}}{\kappa_{b,r} + 1} \frac{1}{\kappa_{b,r} + 1} \sum_{n=1}^N |\rho_n^k|^2 + \left( \frac{1}{\kappa_{b,r} + 1} \right)^2 \\
& \quad \times \left( 2 \sum_{n=1}^N |\rho_n^k|^2 + \right. \\
& \quad \left. \sum_{n_1=1}^N \sum_{n_2 \neq n_1}^N \left( \rho_{n_1}^k e^{j\phi_{n_1}^k} \right) \left( \rho_{n_2}^k e^{j\phi_{n_2}^k} \right)^H \right) \\
& +2 \frac{\kappa_{b,r}}{\kappa_{b,r} + 1} \frac{1}{\kappa_{b,r} + 1} \left( \zeta \sum_{n=1}^N \left( \rho_n^k e^{j\phi_n^k} \right)^H \right)
\end{aligned} \tag{86}$$

where  $\xi_9 = |\bar{\mathbf{g}}_{b,r} \Theta \bar{\mathbf{g}}_{b,r}^H|^2$  and  $\zeta = \bar{\mathbf{g}}_{b,r} \Theta \bar{\mathbf{g}}_{b,r}^H$ .

#### APPENDIX D

From  $\mathcal{E}[R_{u_{2u}}]$  expression presented in Theorem 4, we can find that

$$p_{u_{2u}} = P_{b_1} R_{u_{th}} \frac{y_{2u_{2u}}}{x_{1u_{2u}}} + P_{b_2} R_{u_{th}} \frac{y_{2u_{2u}}}{x_{1u_{2u}}} + R_{u_{th}} \frac{V}{x_{1u_{2u}}} + R_{u_{th}} \frac{\sigma_b^2}{x_{1u_{2u}}} \tag{87}$$

From  $\mathcal{E}[R_{u_{2d}}]$  expression presented in Theorem 2 we can find

$$P_{b_2} = R_{d_{th}} P_{b_1} \frac{x_{1u_{2d}}}{x_{1u_{2d}}} + R_{d_{th}} p_{u_{1u}} \frac{y_{1u_{2d}}}{x_{1u_{2d}}} + R_{d_{th}} p_{u_{2u}} \frac{y_{2u_{2d}}}{x_{1u_{2d}}} + R_{d_{th}} \frac{\sigma_{u_{2d}}^2}{x_{1u_{2d}}} \tag{88}$$

$$P_{b_2} = P_{b_1} a_1 + R_{d_{th}} p_{u_{1u}} a_2 + a_3 \tag{89}$$

where  $a_1 = \frac{\left( \frac{R_{d_{th}} x_{1u_{2d}} + R_{u_{th}} R_{d_{th}} \frac{y_{2u_{2d}} y_{2u_{2u}}}{x_{1u_{2d}} x_{1u_{2u}}}}{x_{1u_{2d}}} \right)}{\left( 1 - R_{u_{th}} R_{d_{th}} \frac{y_{2u_{2d}} y_{2u_{2u}}}{x_{1u_{2d}} x_{1u_{2u}}} \right)}$ ,  $a_2 = \frac{y_{1u_{2d}}}{x_{1u_{2d}} \left( 1 - R_{u_{th}} R_{d_{th}} \frac{y_{2u_{2d}} y_{2u_{2u}}}{x_{1u_{2d}} x_{1u_{2u}}} \right)}$  and  $a_3 = \frac{\eta}{\left( 1 - R_{u_{th}} R_{d_{th}} \frac{y_{2u_{2d}} y_{2u_{2u}}}{x_{1u_{2d}} x_{1u_{2u}}} \right)}$ . Since  $p_{u_{1u}} = P_t - \left( p_{u_{2u}} + \sum_{i=1}^2 P_{b_i} \right)$ , we can get

$$P_{b_2} = P_{b_1} a_1 + a_2 R_{d_{th}} P_t - a_2 R_{d_{th}} p_{u_{2u}} - a_2 R_{d_{th}} P_{b_1} - a_2 R_{d_{th}} P_{b_2} + a_3 \tag{90}$$

$$P_{b_2} (1 + a_2 R_{d_{th}}) = P_{b_1} (a_1 - a_2 R_{d_{th}}) + a_2 R_{d_{th}} P_t - a_2 R_{d_{th}} p_{u_{2u}} + a_3 \quad (91)$$

Substituting (87) into (91) we get

$$P_{b_2} = P_{b_1} b_1 + P_t b_2 - b_3 \quad (92)$$

where  $b_1 = \frac{\left( (a_1 - a_2 R_{d_{th}}) - a_2 R_{d_{th}} R_{u_{th}} \frac{y_{2u_{2u}}}{x_{1u_{2u}}} \right)}{\left( (1 + a_2 R_{d_{th}}) + a_2 R_{d_{th}} R_{u_{th}} \frac{y_{2u_{2u}}}{x_{1u_{2u}}} \right)}$ ,  $b_2 = \frac{a_2 R_{d_{th}}}{\left( (1 + a_2 R_{d_{th}}) + a_2 R_{d_{th}} R_{u_{th}} \frac{y_{2u_{2u}}}{x_{1u_{2u}}} \right)}$  and  $b_3 = \frac{a_4}{\left( (1 + a_2 R_{d_{th}}) + a_2 R_{d_{th}} R_{u_{th}} \frac{y_{2u_{2u}}}{x_{1u_{2u}}} \right)}$ . Now, the rate at user 1 to detect user 2 message is

$$\mathcal{E} [\bar{R}_{u_{1d} \rightarrow u_{2d}}] \approx \log_2 \left( 1 + \frac{P_{b_2} x_{1u_{1d}}}{P_{b_1} x_{1u_{1d}} + p_{u_{1u}} y_{1u_{1d}} + p_{u_{2u}} y_{2u_{1d}} + \sigma_{u_{1d}}^2} \right) \quad (93)$$

we can find

$$P_{b_2} = P_{b_1} c_1 + P_t c_2 - c_3 \quad (94)$$

where  $c_1 = \frac{\left( (\hat{a}_1 - \hat{a}_2 R_{d_{th}}) - \hat{a}_2 R_{d_{th}} R_{u_{th}} \frac{y_{2u_{2u}}}{x_{1u_{2u}}} \right)}{\left( (1 + \hat{a}_2 R_{d_{th}}) + \hat{a}_2 R_{d_{th}} R_{u_{th}} \frac{y_{2u_{2u}}}{x_{1u_{2u}}} \right)}$ ,  $c_2 = \frac{\hat{a}_2 R_{d_{th}}}{\left( (1 + \hat{a}_2 R_{d_{th}}) + \hat{a}_2 R_{d_{th}} R_{u_{th}} \frac{y_{2u_{2u}}}{x_{1u_{2u}}} \right)}$ ,  $c_3 = \frac{\hat{a}_4}{\left( (1 + \hat{a}_2 R_{d_{th}}) + \hat{a}_2 R_{d_{th}} R_{u_{th}} \frac{y_{2u_{2u}}}{x_{1u_{2u}}} \right)}$ ,  $\hat{a}_1 = \frac{\left( \frac{R_{d_{th}} x_{1u_{1d}} + R_{u_{th}} R_{d_{th}} \frac{y_{2u_{1d}} y_{2u_{2u}}}{x_{1u_{1d}} x_{1u_{2u}}}}{1 - R_{u_{th}} R_{d_{th}} \frac{y_{2u_{1d}} y_{2u_{2u}}}{x_{1u_{1d}} x_{1u_{2u}}}} \right)}{y_{1u_{1d}}}$ ,  $\hat{a}_2 = \frac{y_{1u_{1d}}}{x_{1u_{1d}} \left( 1 - R_{u_{th}} R_{d_{th}} \frac{y_{2u_{1d}} y_{2u_{2u}}}{x_{1u_{1d}} x_{1u_{2u}}} \right)}$ ,  $\hat{a}_3 = \frac{\hat{\eta}}{\left( 1 - R_{u_{th}} R_{d_{th}} \frac{y_{2u_{1d}} y_{2u_{2u}}}{x_{1u_{1d}} x_{1u_{2u}}} \right)}$ ,  $\hat{a}_4 = \hat{a}_2 R_{d_{th}} R_{u_{th}} \frac{V}{x_{1u_{2u}}} - \hat{a}_2 R_{d_{th}} R_{u_{th}} \frac{\sigma_b^2}{x_{1u_{2u}}} + \hat{a}_3$ , and  $\hat{\eta} = R_{u_{th}} R_{d_{th}} \frac{y_{2u_{1d}} V}{x_{1u_{1d}} x_{1u_{2u}}} + R_{u_{th}} R_{d_{th}} \frac{y_{2u_{1d}} \sigma_b^2}{x_{1u_{1d}} x_{1u_{2u}}} + R_{d_{th}} \frac{\sigma_{u_{2d}}^2}{x_{1u_{1d}}}$ . Now, from (92) and (94)

$$P_{b_1} b_1 + P_t b_2 - b_3 = P_{b_1} c_1 + P_t c_2 - c_3 \quad (95)$$

and

$$P_{b_1} = P_t \frac{(c_2 - b_2)}{(b_1 - c_1)} - \frac{(c_3 - b_3)}{(b_1 - c_1)} \quad (96)$$

Substitute into (92) or (94) we can get

$$P_{b_2} = P_t \left( b_1 \frac{(c_2 - b_2)}{(b_1 - c_1)} + b_2 \right) - b_1 \frac{(c_3 - b_3)}{(b_1 - c_1)} - b_3 \quad (97)$$

By substituting into (87) we can get

$$p_{u_{2u}} = P_t \left( \frac{(c_2 - b_2)}{(b_1 - c_1)} R_{u_{th}} \frac{y_{2u_{2u}}}{x_{1u_{2u}}} + \left( b_1 \frac{(c_2 - b_2)}{(b_1 - c_1)} + b_2 \right) R_{u_{th}} \frac{y_{2u_{2u}}}{x_{1u_{2u}}} \right) + c_4 \quad (98)$$

where  $c_4 = -\frac{(c_3 - b_3)}{(b_1 - c_1)} R_{u_{th}} \frac{y_{2u_{2u}}}{x_{1u_{2u}}} - b_1 \frac{(c_3 - b_3)}{(b_1 - c_1)} R_{u_{th}} \frac{y_{2u_{2u}}}{x_{1u_{2u}}} - b_3 R_{u_{th}} \frac{y_{2u_{2u}}}{x_{1u_{2u}}} + R_{u_{th}} \frac{V}{x_{1u_{2u}}} + R_{u_{th}} \frac{\sigma_b^2}{x_{1u_{2u}}}$ .

The power expressions in (96)-(98) are the same as (37)-(39), after re-naming the variables.

## REFERENCES

- [1] M. Di Renzo, A. Zappone, M. Debbah, M.-S. Alouini, C. Yuen, J. de Rosny, and S. Tretyakov, "Smart radio environments empowered by reconfigurable intelligent surfaces: How it works, state of research, and the road ahead," *IEEE Journal on Selected Areas in Communications*, vol. 38, no. 11, pp. 2450–2525, 2020.
- [2] C. Pan, H. Ren, K. Wang, J. F. Kolb, M. ElKashlan, M. Chen, M. Di Renzo, Y. Hao, J. Wang, A. L. Swindlehurst, X. You, and L. Hanzo, "Reconfigurable intelligent surfaces for 6g systems: Principles, applications, and research directions," *IEEE Communications Magazine*, vol. 59, no. 6, pp. 14–20, 2021.
- [3] A. Salem, K.-K. Wong, and C.-B. Chae, "Impact of phase-shift error on the secrecy performance of uplink RIS communication systems," 2023. [Online]. Available: <https://arxiv.org/abs/2301.00276>
- [4] L. Dai *et al.*, "Reconfigurable intelligent surface-based wireless communications: Antenna design, prototyping, and experimental results," *IEEE Access*, vol. 8, no. 1, pp. 45 913–45 923, 2020.
- [5] S. Zhang and R. Zhang, "Capacity characterization for intelligent reflecting surface aided MIMO communication," *IEEE Journal on Selected Areas in Communications*, vol. 38, no. 8, pp. 1823–1838, 2020.
- [6] J. Zhang, J. Liu, S. Ma, C.-K. Wen, and S. Jin, "Large system achievable rate analysis of ris-assisted MIMO wireless communication with statistical CSIT," *IEEE Transactions on Wireless Communications*, vol. 20, no. 9, pp. 5572–5585, 2021.
- [7] K. Xu, J. Zhang, X. Yang, S. Ma, and G. Yang, "On the sum-rate of ris-assisted MIMO multiple-access channels over spatially correlated Rician fading," *IEEE Transactions on Communications*, vol. 69, no. 12, pp. 8228–8241, 2021.
- [8] K. Zhi, C. Pan, H. Ren, and K. Wang, "Power scaling law analysis and phase shift optimization of ris-aided massive MIMO systems with statistical csi," *IEEE Transactions on Communications*, vol. 70, no. 5, pp. 3558–3574, 2022.
- [9] X. Mu, Y. Liu, L. Guo, J. Lin, and R. Schober, "Simultaneously transmitting and reflecting (star) ris aided wireless communications," *IEEE Transactions on Wireless Communications*, vol. 21, no. 5, pp. 3083–3098, 2022.
- [10] Y. Liu, X. Mu, J. Xu, R. Schober, Y. Hao, H. V. Poor, and L. Hanzo, "Star: Simultaneous transmission and reflection for 360° coverage by intelligent surfaces," *IEEE Wireless Communications*, vol. 28, no. 6, pp. 102–109, 2021.
- [11] B. Zhao, C. Zhang, W. Yi, and Y. Liu, "Ergodic rate analysis of STAR-RIS aided NOMA systems," *IEEE Communications Letters*, vol. 26, no. 10, pp. 2297–2301, 2022.

- [12] H. Liu, G. Li, X. Li, Y. Liu, G. Huang, and Z. Ding, "Effective capacity analysis of STAR-RIS-assisted NOMA networks," *IEEE Wireless Communications Letters*, vol. 11, no. 9, pp. 1930–1934, 2022.
- [13] A. Papazafeiropoulos, Z. Abdullah, P. Kourtessis, S. Kisseleff, and I. Krikidis, "Coverage probability of STAR-RIS-assisted massive MIMO systems with correlation and phase errors," *IEEE Wireless Communications Letters*, vol. 11, no. 8, pp. 1738–1742, 2022.
- [14] Z. Xie, W. Yi, X. Wu, Y. Liu, and A. Nallanathan, "STAR-RIS aided NOMA in multicell networks: A general analytical framework with gamma distributed channel modeling," *IEEE Transactions on Communications*, vol. 70, no. 8, pp. 5629–5644, 2022.
- [15] H. Ma, H. Wang, H. Li, and Y. Feng, "Transmit power minimization for STAR-RIS-empowered uplink NOMA system," *IEEE Wireless Communications Letters*, vol. 11, no. 11, pp. 2430–2434, 2022.
- [16] F. Fang, B. Wu, S. Fu, Z. Ding, and X. Wang, "Energy-efficient design of STAR-RIS aided MIMO-NOMA networks," *IEEE Transactions on Communications*, vol. 71, no. 1, pp. 498–511, 2023.
- [17] J. Chen and X. Yu, "Ergodic rate analysis and phase design of STAR-RIS aided NOMA with statistical CSI," *IEEE Communications Letters*, vol. 26, no. 12, pp. 2889–2893, 2022.
- [18] J. Zuo, Y. Liu, Z. Ding, L. Song, and H. V. Poor, "Joint design for simultaneously transmitting and reflecting (STAR) RIS assisted NOMA systems," *IEEE Transactions on Wireless Communications*, vol. 22, no. 1, pp. 611–626, 2023.
- [19] J. Xu, Y. Liu, X. Mu, R. Schober, and H. V. Poor, "Star-riss: A correlated t and r phase-shift model and practical phase-shift configuration strategies," *IEEE Journal of Selected Topics in Signal Processing*, vol. 16, no. 5, pp. 1097–1111, 2022.
- [20] X. Yue, J. Xie, Y. Liu, Z. Han, R. Liu, and Z. Ding, "Simultaneously transmitting and reflecting reconfigurable intelligent surface assisted noma networks," *IEEE Transactions on Wireless Communications*, vol. 22, no. 1, pp. 189–204, 2023.
- [21] M. Chung, M. S. Sim, J. Kim, D.-K. Kim, and C.-B. Chae, "Prototyping real-time full duplex radios," *IEEE Communications Magazine*, vol. 53, no. 9, pp. 56–64, Sep 2020.
- [22] M. S. Sim, M. Chung, D. Kim, J. Chung, and C.-B. Kim, D. K. andand Chae, "Nonlinear self-interference cancellation for full duplex radios: From link- and system-level performance perspectives," *IEEE Communications Magazine*, vol. 55, no. 9, pp. 158–167, Sep. 2017.
- [23] M. Chung, D. K. Sim, M. S. andKim, and C.-B. Chae, "Compact full duplex MIMO radios in D2D underlaid cellular networks: From system design to prototype results," *IEEE Communications Magazine*, vol. 5, pp. 16 601–16 617, Sep. 2017.
- [24] Y. Cai, M.-M. Zhao, K. Xu, and R. Zhang, "Intelligent reflecting surface aided full-duplex communication: Passive beamforming and deployment design," *IEEE Transactions on Wireless Communications*, vol. 21, no. 1, pp. 383–397, 2022.
- [25] D. Xu, X. Yu, Y. Sun, D. W. K. Ng, and R. Schober, "Resource allocation for irs-assisted full-duplex cognitive radio systems," *IEEE Transactions on Communications*, vol. 68, no. 12, pp. 7376–7394, 2020.
- [26] Z. Peng, Z. Zhang, C. Pan, L. Li, and A. L. Swindlehurst, "Multiuser full-duplex two-way communications via intelligent reflecting surface," *IEEE Transactions on Signal Processing*, vol. 69, pp. 837–851, 2021.
- [27] P. Guan, Y. Wang, H. Yu, and Y. Zhao, "Joint beamforming optimization for ris-aided full-duplex communication," *IEEE Wireless Communications Letters*, vol. 11, no. 8, pp. 1629–1633, 2022.

- [28] P. K. Sharma, N. Sharma, S. Dhok, and A. Singh, "Ris-assisted fd short packet communication with non-linear eh," *IEEE Communications Letters*, vol. 27, no. 2, pp. 522–526, 2023.
- [29] B. Smida, A. Sabharwal, G. Fodor, G. C. Alexandropoulos, H. A. Suraweera, and C.-B. Chae, "Full-duplex wireless for 6G: Progress brings new opportunities with new challenges," *IEEE Journal on Selected Areas in Communications*, vol. 41, no. 9, pp. 2729–2750, Sep. 2023.
- [30] —, "Guest editorial: Full duplex and its applications," *IEEE Journal on Selected Areas in Communications*, vol. 41, no. 9, pp. 2725–2728, Sep. 2023.
- [31] E. Everett, A. Sahai, and A. Sabharwal, "Passive self-interference suppression for full-duplex infrastructure nodes," *IEEE Transactions on Wireless Communications*, vol. 13, no. 2, pp. 680–694, 2014.
- [32] E. Ahmed and A. M. Eltawil, "All-digital self-interference cancellation technique for full-duplex systems," *IEEE Transactions on Wireless Communications*, vol. 14, no. 7, pp. 3519–3532, 2015.
- [33] T. J. Oechtering and M. Skoglund, "Bidirectional broadcast channel with random states noncausally known at the encoder," *IEEE Transactions on Information Theory*, vol. 59, no. 1, pp. 64–75, 2013.
- [34] S. Khisa, M. Almekhlafi, M. Elhattab, and C. Assi, "Full duplex cooperative rate splitting multiple access for a mimo broadcast channel with two users," *IEEE Communications Letters*, vol. 26, no. 8, pp. 1913–1917, 2022.
- [35] Y. Sun, D. W. K. Ng, Z. Ding, and R. Schober, "Optimal joint power and subcarrier allocation for full-duplex multicarrier non-orthogonal multiple access systems," *IEEE Transactions on Communications*, vol. 65, no. 3, pp. 1077–1091, 2017.
- [36] A. Abrardo, M. Moretti, and F. Saggese, "Power and subcarrier allocation in 5g noma-fd systems," *IEEE Transactions on Wireless Communications*, vol. 19, no. 12, pp. 8246–8260, 2020.
- [37] A. Papazafeiropoulos, P. Kourtessis, and I. Krikidis, "STAR-RIS assisted full-duplex systems: Impact of correlation and maximization," *IEEE Communications Letters*, vol. 26, no. 12, pp. 3004–3008, 2022.
- [38] M. Alouini and A. J. Goldsmith, "Area spectral efficiency of cellular mobile radio systems," *IEEE Transactions on Vehicular Technology*, vol. 48, no. 4, pp. 1047–1066, July 1999.
- [39] A. M. Mathai, *An Introduction to Geometrical Probability*, Gordon and Breach Science Publishers.
- [40] M. Abramowitz and I. A. Stegun, *Handbook of Mathematical Functions With Formulas, Graphs, and Mathematical Tabl*, Washington,D.C.: U.S. Dept. Commerce, 1972.